Chapter 5

Improving the quality and reliability of electronic equipment and power systems

5.1. Acoustic emission diagnostics of solder joints on printed circuit boards

Igor Kovtun[1], Vilen Royzman[2], Andriy Voznyak[3]
Khmelnytsky National University, Khmelnytsky, Ukraine
E-mail: [1]*dr.igorkovtun@gmail.com*, [2]*royzman@ukr.net*, [3]*andreyvoznyak27@gmail.com*

Abstract. The paper represents technical diagnostics of printed circuit boards in particular the solder joints performed by commonly used through-hole and surface mount technologies. The research methods involved mechanical tensile and bend tests and acoustic emission method application with simultaneous monitoring both mechanical characteristics and acoustic emission parameters in order to find their correlation. On the base of conducted experiments method for solder joint technical diagnostics by using method of acoustic emission in pure bending cycling tests has been designed.

Keywords: solder joint, printed circuit board, technical diagnostics, electronic component, acoustic emission, tensile test, pure bending.

1. Introduction

Complexity and micro-miniaturization in electronic and computer production technologies constantly increase quality and reliability standards for their components. Printed circuit boards (PCB) are considered the main building blocks of modern electronics, which represent assemblies purposed to electrically connect and, what is also important, mechanically support electronic components. However, operation and even technology cause mechanical interactions and forces, acting between PCB substrate and electronic components, and spreading through their links. Such tensile, shear, bending or torque forces cause strain and stress in substrates, which are subsequently transmitted to bodies of components through the contact joints that appear to be the weakest links in the assembly. The damages of the joints cause failures of the whole electronic units and therefore require detailed studying.

The general technology for components installation (e.g. capacitors, resistors or active devices) on PCBs remains soldering although quality of soldered joints (SJ) is not always achievable due to numerous defects. Therefore, one of the primary tasks to provide reliability to SJs is to apply and improve their testing methods. The range of methods for non-destructive or destructive SJ tests provided by the state standard [1, 2] does not always provide proper quality selection. Since soldered joint strength is one of the indicators applied to assess its quality, development of methods for strength diagnostics of soldered joints on PCBs is the objective for the current research.

The diagnostics of SJs wad performed for two commonly used technologies: through-hole technology (THT) and surface mount technology (SMT). The research methods involved static mechanical tensile and bend tests and acoustic emission (AE) method application with simultaneous monitoring both mechanical characteristics and acoustic emission parameters.

2. Nondestructive evaluation methods

Application of electrical and physical methods for SJ quality control attracts close attention in nowadays. In accordance to [2] these methods include: electro-parametric, noise, acoustic emission, exoelectronic emission, photovoltaic and recombinant radiation methods. Among these methods, the most of which have range of intrinsic disadvantages such as high cost and complexity of measuring instrumentation, the method of acoustic emission has recently hastened its growth due to its high applicability for nondestructive diagnostics and prediction of strength of technical objects in general and of solder joints in particular. Table 1 shows the list of characteristics represented for comparison of acoustic emission methods with another nondestructive evaluation (NDE) methods.

Table 1. Comparative characteristics of acoustic emission methods against other NDE methods

Acoustic emission method	Other NDE methods
Detects defects in progression	Detect geometry of defects
Requires load testing	Does not require load testing
Each test is unique	Tests are replicable
Sensitive to material consistency	Less sensitive to material consistency
Less sensitive to geometry of tested object	More sensitive to geometry of tested object
Simplicity of application	Complexity of application
Transducers require minor contact area for attachment on the tested object	Require reach to the full surface of tested object
The object is completely monitored by the single test	Subsequent monitoring parts of the object
Difficulties: sensitive to noise	Difficulties: object geometry dependent

Comparative analysis of NDE indicates in favor of acoustic emission method as versatile, simple and inexpensive method applicable to assessment of health conditions of the structures.

By the definition, acoustic emissions are pressure waves generated due to transient release of energy when a material is subjected to mechanical (in this case), thermal or chemical changes causing irreversible deformations or changes in atomic arrangement. The energy released travels as a spherical wavefront and is converted to electrical signal by transducers placed on the surface of the material (Fig. 1). The transducer output is filtered and amplified to eliminate ambient noise and increase the signal-to-noise ratio.

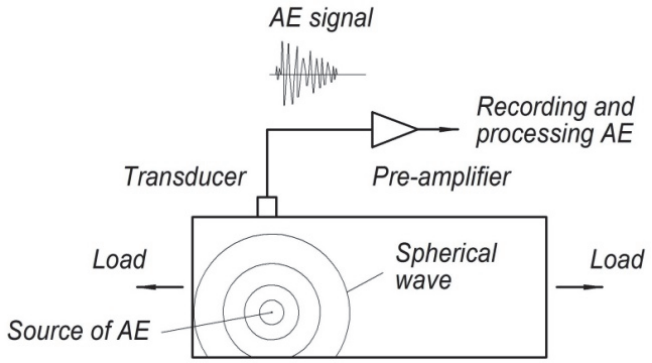

Fig. 1. The basic principle of acoustic emission generation and recording

The output signal of transducer represents high frequency oscillation (Fig. 2). The single and unique signal is named as the event of acoustic emission and assumed as the total amount of all oscillations received within time interval of 1 ms.

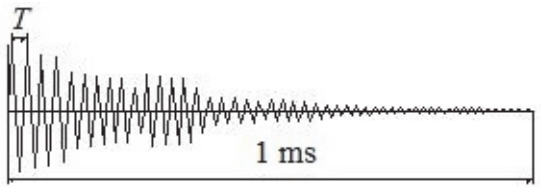

Fig. 2. Acoustic emission event image

Every event is approximated by the expression:

$$U = Ae^{-nt}\sin\omega t, \quad (1)$$

where A – amplitude; n – attenuation factor (factor which is determined by damping characteristics of the structure); ω – cycling frequency; t – time:

$$\varpi = \sqrt{p^2 - n^2}, \tag{2}$$

where:

$$p = c/m, \tag{3}$$

where c – rigidity (static force that causes single displacement); m – reduced mass. Normally $n \ll m$ and $\omega = p$.

Oscillation is characterized by its period:

$$T = \frac{2\pi}{\sqrt{p^2 - n^2}} \approx \frac{2\pi}{p}. \tag{4}$$

For the analysis high frequency signal (Fig. 3(a)) received from the transducer is then processed to select oscillations (Fig. 3(b)), whose amplitudes exceed discrimination threshold of the amplifier, and then events. An event is considered as collection of oscillations, received within time period of 1 ms, and then converted into one impulse (Fig. 3(c)) of amplitude equal to maximal amplitude of oscillations collected.

The common parameters obtained by processing AE are: cumulative count of oscillations; time rate of oscillation count (count rate); cumulative count of events (total count); time rate of events count (activity) Eq. (5); amplitude of events; linear coordinate of events, which is calculated by using Doppler effect of time difference in signal arrivals to two transducers $\Delta t = t_2 - t_1$ (Fig. 3(d)); power of events Eq. (7) and energy of events Eq. (8).

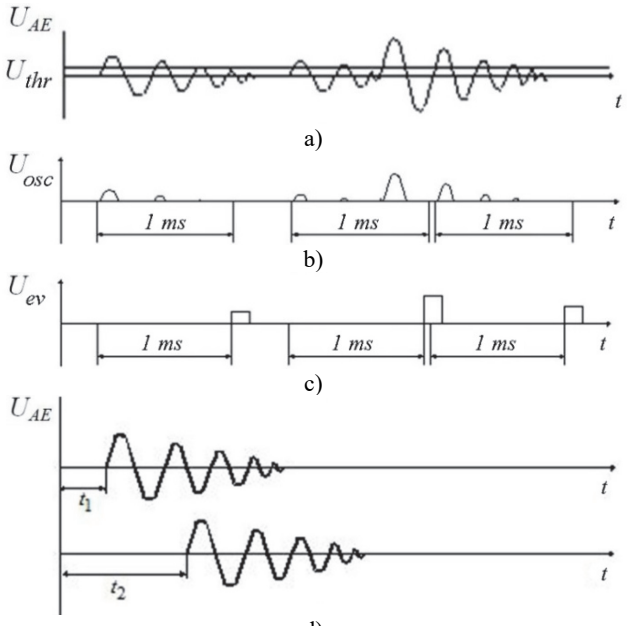

Fig. 3. Acoustic emission processing: a) high frequency oscillation, b) oscillations selected, c) events converted, d) using Doppler effect for linear location

Acoustic emission activity represents time rate of signals count:

$$N = \frac{N_c}{T}, \tag{5}$$

where N_c – signals count; T – time.

Power or electric power of events transduced by the piezoelectric sensor is expressed by formula:

$$W = k \lim_{T \to \infty} \frac{1}{T} \int_0^T U^2(t) dt, \tag{6}$$

where k – proportionality factor; T – time interval; $U(t)$ – amplitude of event.

Power of event is processed by measuring instrument as:

$$W = U^2 N_o, \tag{7}$$

where U – amplitude of event, N_o – oscillation count per event, which is directly proportional to event duration.

Acoustic emission energy is defined by the formula:

$$E = k \frac{\sum_{i=1}^{N_c} W_i}{T}, \tag{8}$$

where k – proportionality factor; W_i – power of event.

3. Acoustic emission measuring station

Acoustic emission station was designed in experimental laboratory of the static and dynamic strength in electronics in Khmelnytsky National University [3]. The station structure is shown in Fig. 4.

The station is created to perform online reading, saving and processing of acoustic emission parameters, received due to static and dynamic mechanical tests of the structures.

In the represented research the station was used for experimental and applied diagnostics and predicting strength of solder joints on printed circuit boards subjected to the following tests:

- Static tests conducted by tension test machine IR 5057-50;
- Dynamic tests conducted by the shaker VEDS 200;
- Thermal tests conducted in climatic chamber Feitron 3526/51.

Reading and initial processing of acoustic emission signals is performed by acoustic emission measuring instrument AF-15. Signals are transduced by the piezoelectric sensors. Final processing of the data is performed by personal computer connected to AF-15 via the designed unit of parallel input/output interface.

The following improvements have been made to create AE measuring station:

- Modification of sub-units of linear coordinates, amplitude and adder in measuring instrument AF-15;
- Design of parallel input/output interface;
- Development of the software for processing acoustic emission data.

4. Solder joint defects

Soldering, in which two or more items are joined together by melting and putting a filler metal (solder) into the joint, is a complex technology involving physical and chemical processes, which pass through solid, liquid and gaseous phases [1, 2]. The objectives of represented research are

two commonly used technologies: through-hole technology (THT) and surface mount technology (SMT).

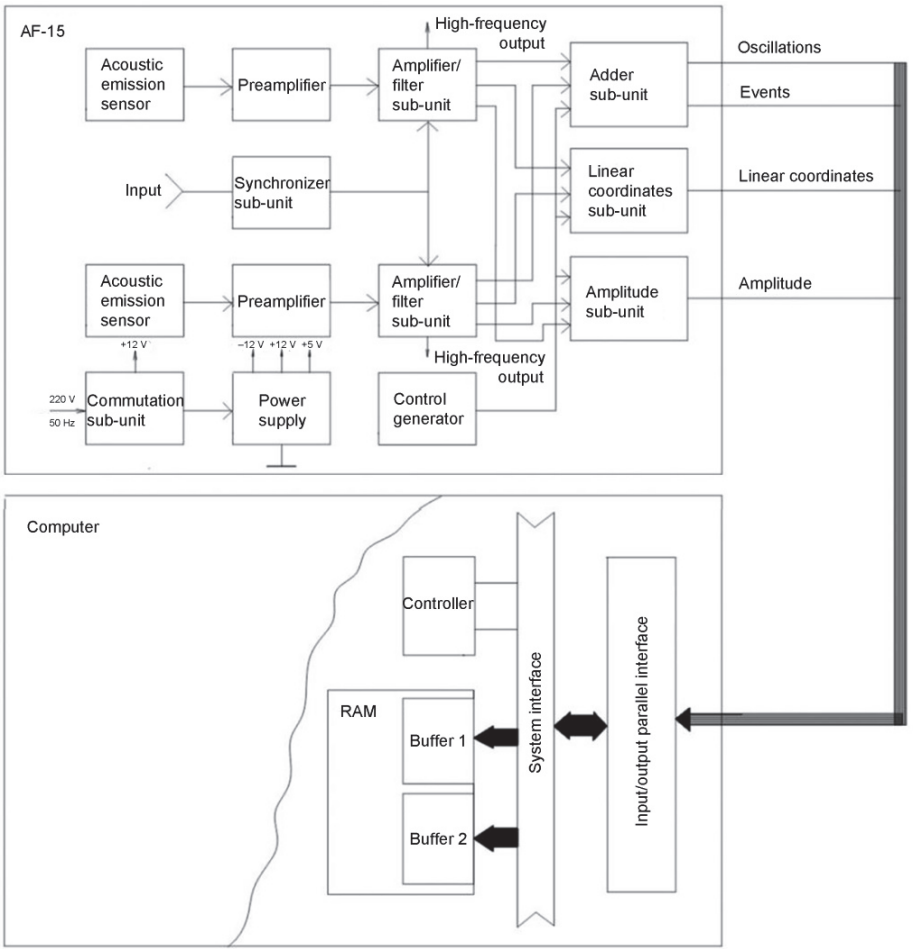

Fig. 4. Acoustic emission measuring station structure

Through-hole technology consists in mounting electronic components by leads inserted through holes on one side of the board and soldered onto copper traces on the other side. Boards may be single-sided, with an unplated component side, or more compact double-sided boards, with components soldered on both sides. Horizontal installation of through-hole parts with two axial leads (such as resistors, capacitors, and diodes) is done by bending the leads 90 degrees in the same direction, inserting the part in the board (often bending leads located on the back of the board in opposite directions to improve the part's mechanical strength), soldering the leads, and trimming off the ends. Leads may be soldered either manually or by a wave soldering machine.

In surface-mount technology components are mechanically redesigned to have small metal tabs or end caps that could be soldered directly onto the PCB surface, instead of wire leads to pass through holes. Components are much smaller and component placement on both sides of the board is more common than with through-hole mounting, allowing much smaller PCB assemblies with much higher circuit densities.

Solder joints remain the general technology for components installation, although their quality is not always achievable due to numerous defects.

One of the main parameters used to assess quality of solder joints is the mechanical

characteristics – strength, in particular tensile and shear ultimate strength. The strength of solder joints depends on large amount of design and technology factors and thus is determined by ability of the weakest link in the structure to resist destruction. The majority of solder joint defects are represented in Table 2.

Table 2. Types of solder joint defects

Defect	Description
Absence of solder	Solder is absent in a joint
Underheated solder	Underheating solder while joining
Cold joint	Leads mechanical displacement while solidifying
Grainy joint	Solder contamination causing grains
Excessive solder	Excessive amount of solder what complicates applying SJ tests
Solder starved	Solder amount is insufficient for reliable joint
Low wetting pad	Solder fail to wet to the contact pad
Low wetting pin	Solder fail to wet to the lead
Solder icicle	Sharp peaks on the solder surface
Piercing	Small holes on the solder concave surface
Hollows	Large holes in solder to expose on the surface
Recess	Holes or other solder damages penetrating down to joint bottom
Oil inclusions	Oil drops in the joint
Solder bridge	Unintended connection between pins
Solder beads	Solder beads of various diameter on PCB surface
Solder spatters	Solder spatters on PCB surface
Internal hollows	Hollows inside a solder not exposed to surface
Contamination and foreign particles	Solder surface is contaminated what limits its control
Flux remainders	Flux remainders on the solder surface what worsens connection
Low-quality pins	Leads are too short or long, improperly bent (deformed), not coplanar
Low filling	The contact hole is completely or partially unfilled with the solder
Low adhesion	The solder is completely or partially not adhered to the basic material
Porousness	Residual, soldering, diffusive porousness
Solder erosion	Dissolving basic material by contacts with liquid solder
Solder notch	Local erosion
Solder tear	The foil is detached from PCB substrate as overheated; contact is torn a part
Solder jumpers	Short connection between elements as soldered
Solder contamination	Accumulation of foreign inclusions in soldering tab
Low solder area	Area to be soldered is insufficiently covered with solder (depends on surface preparation)
Solder joint exfoliation	Solder and contact pad are detached from PCB substrate as overheated

5. Through-hole technology

Solder joints of MLT2 resistors produced by THT technology were the objectives for the research. The research was conducted in progress of strain analysis presented in [4] and aimed at assessing SJs strength by using tensile tests and acoustic emission method.

In order to assess acoustic emission signals against types of defects and find their possible correlation tests were performed for solder joints, part of which was soldered with implemented defects.

Static mechanical tensile tests were conducted for SJs installed on the PCBs into 2 mm contact pads. For experiments the tensile machine IP-5057-50 with 500 N ultimate load was used. The load measurement tolerance was under 1 % of maximal load. To perform the test one lead of a resistor was soldered to metallized hole in PCB with tin-lead alloy and fixed in the upper clamps of tensile machine. PCB was firmly fixed in custom lower clamps of the machine. The load scheme

is shown in Fig. 5.

60 solder joints were tested: 20 SJs had no defects; 20 SJs had "cold solder" defect; 20 SJs had "low solder adhesion" defect. The load was applied with the constant speed at 0.1 mm per minute. During the test the following AE parameters were recorded: amplitude; activity; total count.

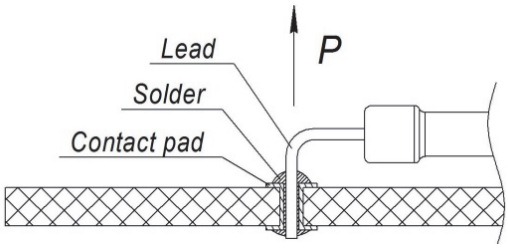

Fig. 5. Load application in solder joint tensile test

First experiments indicated the lowest tensile strength for SJs having "low solder adhesion" defect. The ultimate load for the joints with such defects was 30-40 N. Fatal damages of these joints occurred when the leads were pulled out of the solder with no acoustic emission detected. Since the case when leads are not wetted completely is very unlikely, further studying SJs with partly wetted leads were considered to be more reasonable.

The averaged results of the experiments are given in Table 3. Statistical analysis of experimental data testified of significant decreasing ultimate load for defective SJs with 95 % confidence probability.

Table 3. Tensile test results for soldered joints of 60 resistors MLT 2

Group	Solder joint condition	Average ultimate load, N	Average strength decrease, %
1	No defect joint	116.2	–
2	Cold joint	44.5	62
3	Low adhesion joint	75.9	35

During the tests AE parameters were recorded along with the load progression. AE data analysis resulted in total count N (impulses, imp) and maximal activity Amax (impulses per second, imp/s) measured for different types of SJs during their tensile tests. Acoustic emission parameters were recorded in the load range from 0 to 44 N what corresponds to average ultimate load for the cold joints and makes 40 % of ultimate load for no defect joints (Table 4, Fig. 6).

Table 4. Acoustic emission parameters under 40 % of solder joint ultimate tensile load

Group	Solder joint condition	Total count, imp	Maximal activity, imp/s
1	No defect joint	34	51
2	Cold joint	70	210
3	Low adhesion joint	22	40

As foreseen, the AE character differed for different defects. Fig. 6 demonstrates acoustic emission diagrams produced by the load progression applied during tensile tests for three groups of SJs with mentioned types of defects.

Analysis of acoustic emission detected along the tests shows sensitivity and applicability of this method to detect defects in SJs and even assess their strength. Besides, it holds potential for nondestructive diagnostics of solder joints long before the final destruction.

6. Surface mount technology

The metallic ceramic capacitors K10-17B and K10-50B, which are surface mount devices (SMD), were objectives for the next research. Nowadays SMD technology gains popularity due

to range of advantages before THT. Exploring, assembling and testing these capacitors are likely to cause damages in form of contact pads defoliation and detachments or even capacitor destruction [5]. Preliminary shear strength tests revealed that ultimate shear loads 2-4 times exceed tensile ones. Therefore, capacitors K10-17B and K10-50B were subjected to the tensile tests aimed at defining: ultimate loads that cause mentioned damages; tensile strain of capacitors; difference in ultimate loads for overheated solder and cold solder joints of K10-50B capacitors; correlation between AE signals and solder joint strength for varied technological conditions.

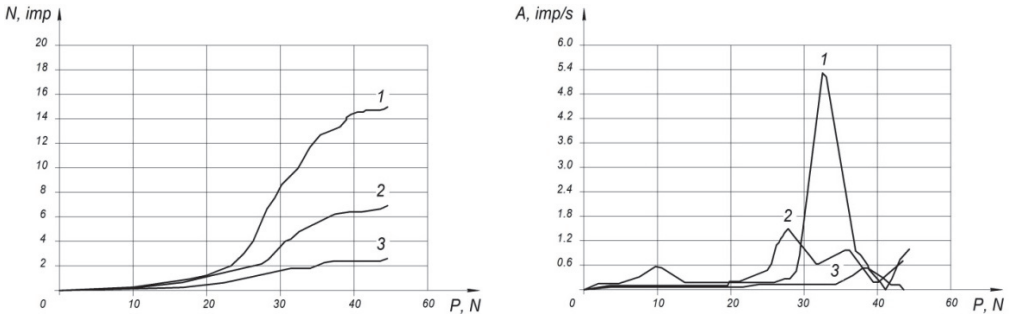

a) b)

Fig. 6. Acoustic emission – load diagrams during tensile tests of three types of solder joints: 1 – cold joints, 2 – low solder adhesion joints, 3 – solder joints without defects

In order to minimize errors in measuring small loads for tensile tests the special appliance was designed (Fig. 7).

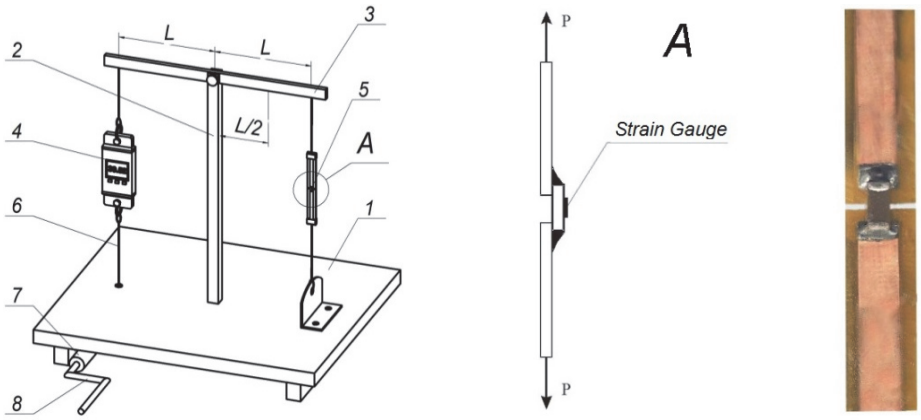

a) b) c)

Fig. 7. Manual tensile test appliance: a) structure, b) strain gauge attachment, c) capacitor installation: 1 – base; 2 – support, 3 – lever, 4 – dynamometer, 5 – capacitor, 6 – traction, 7 – drum; 8 – handle

The measuring train used in the test consisted of electro-tensometry and acoustic emission instruments. Two batches of 100 capacitors K10-17B and K10-50B were tested. Capacitors 5 (Fig. 7) were soldered by their termination caps to the ends of two strips, cut out of the PCB substrate, which were then clamped in between the lever 3 and the base 1. Turning handle 8 revolved the drum 7 and through the traction 6 pulled the left side of the lever 3 so as to apply load to capacitors; load was indicated by dynamometer 4. To increase measurement accuracy for smaller loads the testing appliance is designed so that lever shoulders can be varied if needed.

Tests were conducted with simultaneous records of acoustic emission and loads. In all the cases destruction occurred as defoliation of a contact pad. Strain gauges were attached to capacitors (Fig. 7) with purpose to define strain versus load dependences (Fig. 8). The average

ultimate loads measured for batches of capacitors K10-17B and K10-50B made $P_1 = 23.7$ N and $P_2 = 31.8$ N correspondently.

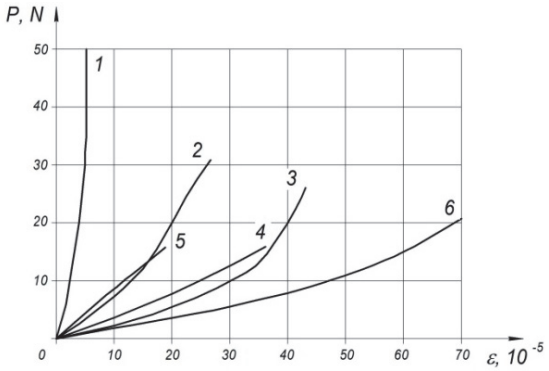

Fig. 8. Strain versus tensile load dependences for capacitors K10-17B (1) and K10-50B (2, 3-6)

The next experiment was conducted to verify the overheating effect to ultimate load of solder joints. Two groups of capacitors K10-50B that differed in soldering technologies were subjected to tensile tests. In the first group soldering was conducted at 220-270 °C temperature during 10 s with standard alloy POS-61, in the second group – at 94-120 °C temperature with rosin alloy.

Data analysis (table 1) testified that overheating of solder joints improves their adherence to the contact pads and increases their tensile strength.

Significant difference between cold solder and overheated joints was indicated by acoustic emission recorded (Fig. 9) during experiment. For the cold solder AE signals appeared earlier; their total count was 1.5 times and activity – 2.5 times higher than for overheated ones. Average strains recorded for cold solder and overheated joints were $\varepsilon_1 = 70\times10^{-5}$ and $\varepsilon_2 = 45\times10^{-5}$ correspondently.

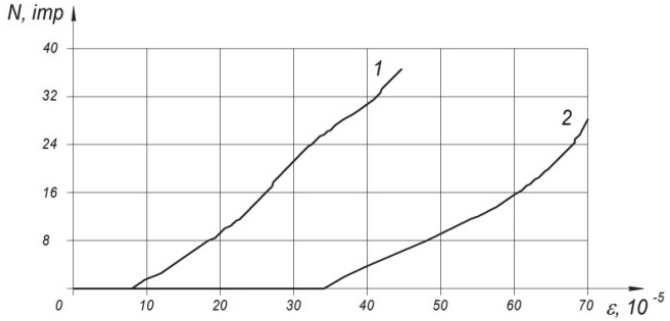

Fig. 9. Acoustic emission total count versus strain diagrams:
1 – cold solder joints with ROSE alloy, 2 – overheated joints with POS-61 alloy

The next experiment was made with conjecture that contact joint strength depends on soldering temperature. The experiment was arranged with account for limitations posed by complexity to measure solder temperature either theoretically or practically. The decision was made to remain soldering technology unchanged with an exception for contact joint temperature, which was considered to increase by preliminary heating the capacitors.

The experiment was conducted for two groups of capacitors. 1st group was soldered at the standard temperature. 2nd group was preheated before soldering in thermostat within 1 hour at the discrete temperatures: 150 °C, 180 °C, 200 °C, 215 °C, 230 °C, 250 °C. After preheating capacitors were soldered and subjected to tensile tests by the method explained above.

Data analysis (Table 5) indicated that preheating of solder joint at 200 °C increased its strength

by 50 %. Moreover, optimal preheating temperature, producing maximal strengthening effect was defined in interval of 180-200 °C.

Table 5. Tensile ultimate loads of K10-50B capacitor solder joints for different temperature modes

Soldering technology modes					
Duration: 10 s		Duration: 3 s			
POS 61 t = (220-270) °C	Rosin alloy t = (94-120) °C	Standard	Preheated in thermostat within 1 hour at the temperatures, °C		
			150	200	250
Average tensile ultimate loads, N					
59.7	36.2	30.6	40.3	47.6	22.9

7. Pure bending theoretical model

Conducting tensile tests with simultaneous recording acoustic emission showed perspectives for nondestructive strength diagnostics of components solder joints installed on PCB, although practical application of the method was limited by monitoring only the single component joints at the time. In order to overcome this limitation and conduct tests for entire PCB with all components installed the pure bending technique was applied (Fig. 10). The pure bending was designed to provide equal testing stress over the PCB area as applied in between two supports. Thus, all SJs installed within the tested area can be monitored simultaneously.

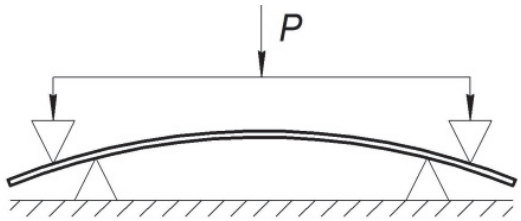

Fig. 10. Pure bending load scheme

PCBs populated with components installed by SMD technology were now the research objectives. SJ strength assessment considers solder mechanical characteristics, which are specified with consideration of design and technology of the joint. The strength of low-melting solders in cast phase is less than that of SJ. The lowest level of ultimate strength for solder POS40 in the cast phase is $\sigma_u = 40$ MPa [6].

The ultimate strength for fiberglass substrate is $\sigma_u = 45$-100 MPa.

Assuming ultimate strength of the solder as the reference value the test stress is calculated by the formula:

$$[\sigma] = \frac{\sigma_u}{n} = \frac{40}{2.5} = 16 \text{ MPa}. \quad (9)$$

where σ_u – ultimate strength, $n = 2.5$ – safety factor.

The possible inaccuracy entailed by no account for design and technology of the joint will deposit into the safety factor. Obtained safety factor is sufficient to provide safe testing stress σtest within proportionality strain area of solder material, so that solder is subjected to only elastic deformations, which do not reduce its strength.

Then the load P applied to PCB is specified for the nondestructive tests. Load application scheme for PCB test is shown in Fig. 11.

Maximal stress [6] is produced in dangerous part of PCB cross section – in peripheral layer, where bending moments are maximal $M = M_{max}$. In pure bending area with length L which is created by and lays in between two supports A and B, maximal stress is found by formula:

$$\sigma_{max} = \frac{M_{max}}{I_{ax}} y_{max}, \tag{10}$$

where M_{max} – maximal bending moment produced by load P; I_{ax} – axial moment of inertia; y_{max}– maximal distance from the neutral line of the cross-section to the peripheral layer (fibers); $y_{max} = h/2$, where h – thickness of PCB substrate.

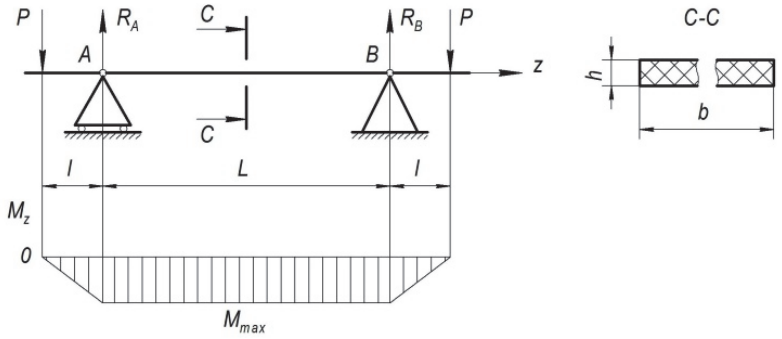

Fig. 11. Load application and diagram of internal bending moments in PCB

Since ratio I_{ax}/y_{max} $\frac{\mathrm{I_{oc}}}{\mathrm{y_{max}}}$represents axial moment of resistance W_{ax}, Eq. (2) will be shortened to:

$$\sigma_{max} = \frac{M_{max}}{W_{ax}}. \tag{11}$$

As required by strength condition of normal stress under bending load – maximal stress produced by the applied load should comply with acceptable standard $[\sigma]$:

$$\sigma_{max}\ [\sigma]. \tag{12}$$

Performing nondestructive tests to PCBs requires maximal acceptable load estimation.

Using Eqs. (3) and (4) for which in accordance to load application scheme (Fig. 11) maximal bending moment equals:

$$M_{max} = P \cdot l, \tag{13}$$

and axial moment of resistance of rectangular section [6] is expressed as:

$$W_{ax} = \frac{b \cdot h^2}{6}. \tag{14}$$

Maximal acceptable load for nondestructive bending tests of PCBs should comply with condition:

$$[P] \leq \frac{b \cdot h^2}{6 \cdot l} [\sigma]. \tag{15}$$

8. Pure bending static tests

Pure bending tests conducted by tensile machine IP-5057-50 indicated that the activity of acoustic emission responds to the loading speed. Since AE data analysis requires its essential

amount the decision was made to conduct tests at maximal acceptable loading speed 100 millimeters per minute. The load was applied under acceptable limit calculated by Eq. (3) $P_{test} = 36$ N.

However single load did not produce considerable activity of AE signals yet and testing was considered to conduct in multiple load and unload cycles. Each PCB was tested in 5 cycles. Minimal and maximal stresses in cycles equaled $\sigma_{min} = 0$ MPa and $\sigma_{max} = 16$ MPa correspondently. Acoustic emission was recorded during all the tests by piezoelectric gauges and via pre-amplifiers at frequency band of 0.02-0.2 MHz. The gauges were attached to PCB surface through the layer of acoustic paste.

The tests were conducted for 60 double sided fiberglass foil laminated PCBs (320×120×1.5×0.1 mm size). For the experiment PCBs were prepared and sorted into three equal groups by defects embedded into their solder joints: 1) PCBs with no defects; 2) PCBs with cold joint defects; 3) PCBs with low solder adhesion defects. Each PCB was populated with one component – resistor MLT-2. In group 1 resistors were installed in compliance with technological standard [7]. In group 2 one of the resistors' leads was mounted to PCB as a cold joint, in particular as "circle crack" joint which is likely for soldering technology. In the group 3 low solder adhesion defects were embedded into solder joints for what resistors' leads had not been wetted before soldering.

During the tests the following AE parameters [8] were recorded: amplitude; activity; total count. The test results indicated that PCBs with no defect solder joints do not radiate acoustic emission during all cycles. The total count of SJs with low solder adhesion defects made 10-15 imp with amplitude 1 mV. Normally such signals are radiated at load progression and in the moments of maximal load. Signals radiated by cold joint defects are characterized by considerably higher total count (30-40 imp) with amplitude up to 3 mV. The specificity of cold joints is that AE appears on load discharging phase of cycles, what can be explained by cracks converging their edges. Figs. 12, 13 demonstrate acoustic emission – cycling load diagrams recorded during pure bending tests of PCBs with embedded solder joint defects.

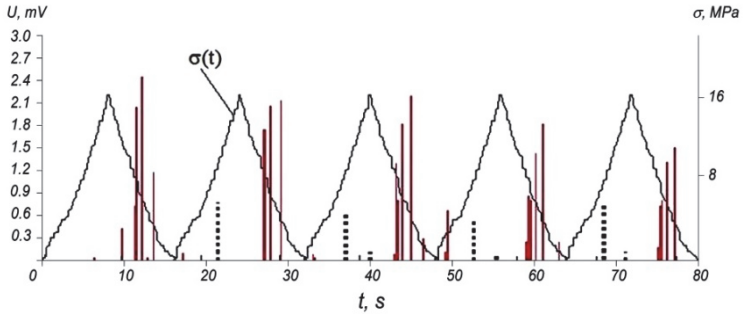

Fig. 12. Acoustic emission amplitude – cycling load diagram: solid line – low solder adhesion, dash line – cold joint

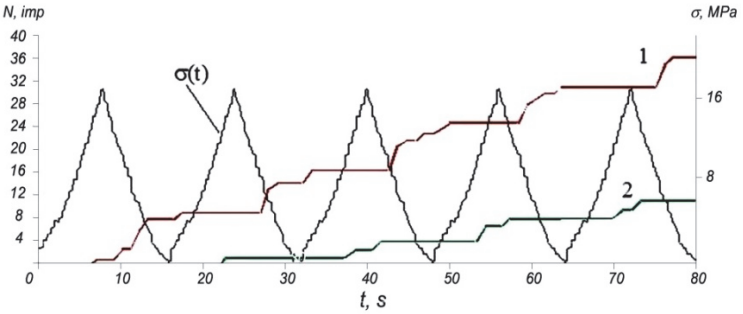

Fig. 13. Acoustic emission total count – cycling load diagram: 1 – cold joint, 2 – low solder adhesion

AE data analysis indicated total count as the most informative parameter to correlate with various types of solder joint defects. Conducted experiments give the reason to use identified character of acoustic emission to develop methods for strength diagnostics of solder joints on printed circuit boards.

9. Theoretical model of planar defect location

The location accuracy of acoustic emission is strongly effected by acoustic characteristics of the transmitting medium and becomes complicated problem for a medium which is heterogeneous. So, AE spreading and location in PCBs is strongly complicated due to structural complexity of PCBs, that consist of THT or SMD components, conductive tracks, pads and other features etched from copper sheets laminated onto a non-conductive substrate, whose acoustic characteristics (Table 6) are different. The task of the current research was to develop method for planar location of AE whose sources are defects progressing in stressed PCBs when exposed to external forces.

Table 6. Acoustic characteristics of PCB structural materials

Material	Density $\rho \cdot 10^3$, kg/m^3	Wave speed $v \cdot 10^3$, m/s			Attenuation constant δ, m^{-1}
		Longitudinal	Cross	Surface	
Textolite	1.2–1.3	2.63	–	–	> 100
Lead	11.4	2.16	0.70	0.63	1-10
Copper	8.9	4.66	2.26	2.12	10-100

The idea of the method developed for planar location consisted in remote detection of AE by piezoelectric transducers through the volume of homogeneous medium [10, 11] such as water, unlike detecting AE on the PCB surface where AE signal is likely to be distorted or even lost. Water retains the most acceptable attenuation constant $\delta = 2.5$ as compared to other homogeneous mediums.

The testing installation represents load appliance for PCBs and 4 piezoelectric sensors installed inside the water chamber. PESs were installed on the plane parallel to PCB at the specified distance, so that their receiving side faced the tested PCB. Acoustic waves generated by defects in PCB spread through the volume of water and reach the sensors with negligible loss or distortion.

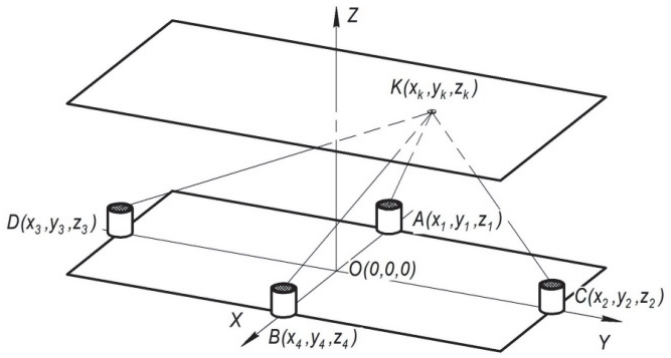

Fig. 14. Planar location scheme in acoustically transparent medium:
K – source of AE; A, B, C, D – piezoelectric sensors

The planar location in Cartesian coordinates is calculated in the space coordinate system XYZ. 4 PESs are installed on the axes X and Y in $z = 0$ plane (Fig. 14).

The monitored PCB lays in the plane $z = zK$, where zK is distance between the PCB and PESs. The 4 channel acoustic emission system detects two time differences τ_1 and τ_2 of signal arrivals to two pairs of opposite sensors in two orthogonal axes. Time differences τ_1 and τ_2 is related to distance differences from AE source K to PESs in correspondent pair:

$$\begin{cases} BK - AK = \tau_1 \vartheta, \\ CK - DK = \tau_2 \vartheta. \end{cases} \tag{16}$$

where τ_1 – time difference of signal arrivals to PESs in points A and B; τ_2 – time difference of signal arrivals to PESs in points C and D; υ – ultrasonic speed in water.

The final expressions for AE coordinate calculation are represented as:

$$\begin{cases} x_k = \pm \frac{1}{2} \sqrt{\frac{\tau_1^2 \vartheta^2 \tau_2^2 \vartheta^2 (\tau_2^2 \vartheta^2 - \tau_1^2 \vartheta^2 + 4x_4^2 - 4y_2^2) + 4\tau_1^2 \vartheta^2 y_2^2 (\tau_1^2 \vartheta^2 - 4x_4^2 - 4z_k^2)}{4\tau_1^2 \vartheta^2 y_2^2 + 4\tau_1^2 \vartheta^2 x_4^2 - 16 x_4^2 y_2^2}}, \\ y_k = \pm \frac{1}{2} \sqrt{\frac{\tau_1^2 \vartheta^2 \tau_2^2 \vartheta^2 (\tau_1^2 \vartheta^2 - \tau_2^2 \vartheta^2 + 4x_4^2 - 4y_2^2) + 4\tau_2^2 \vartheta^2 x_4^2 (\tau_2^2 \vartheta^2 - 4y_2^2 - 4z_k^2)}{4\tau_1^2 \vartheta^2 y_2^2 + 4\tau_2^2 \vartheta^2 x_4^2 - 16 x_4^2 y_2^2}}. \end{cases} \tag{17}$$

In Eq. (9) positive or negative signs are selected regarding sings of τ_1 and τ_2.

The experimental verification of the offered method was conducted in testing installation with PESs installed at 70 mm distance from the tested PCB. The AE planar location diagrams obtained by regular surface location performed on the PCB surface and by the developed method are shown in Fig. 15(a) and Fig. 15(b) correspondently.

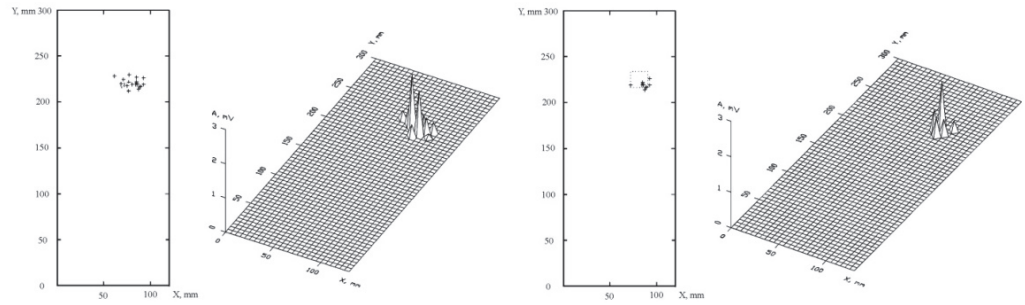

a) b)

Fig. 15. Acoustic emission planar diagrams recorder during PCB bending tests:
a) location on PCB surface, b) location in acoustically transparent medium

The application of developed method in acoustically transparent medium indicated that located area of the defect makes about 1 % of the total PCB area, what provides accuracy 2-4 time higher than by the regular surface location.

10. Method for technical diagnostics

1. Printed circuit boards are tested by pure bending load under acceptable limit specified by the safety factor for solder material $n = 2.5$.

2. In case acoustic emission is detected, test is repeated in 5 load/unload cycles. Acoustic emission progression during cycle test indicates of solder joint defect and such PCB is rejected and classified as joint with growing defect.

3. When required defect location is performed in order to repair it.

The developed method has been tested out on the batch of industrial printed circuit boards. The tests were conducted for 32 single sided fiberglass foil laminated PCBs (120×140 mm size). During tests acoustic emission was detected for three PCBs what indicated progressing defects. Analysis of AE character identified type of the detected defects – low solder adhesion, which was then proved by detailed optical 10x zoom revision of rejected PCBs in places where AE was located. Defects were also tested by passing electric current through the defected solder joints and

measuring their electric resistance. Since PCBs had been used for a long time before the tests and identified defects had remained hidden so they can have developed during their further operation and would have caused a failure of the whole electronic unit.

11. Conclusions

Strength diagnostics conducted for solder joints performed by through-hole and surface mount technologies on printed circuit boards by using methods of mechanical tensile and pure bending tests and method of acoustic emission with simultaneous monitoring both mechanical characteristics and acoustic emission parameters allowed to find the relationship between parameters of acoustic emission and such defects of solder joints as “cold joint” and “low solder adhesion”.

Surface mount technology has been optimized by introducing solder joints preheating that results in 50 % strengthening effect in the temperature interval of 180-200 °C.

The theoretical model of pure bending condition for printed circuit boards has been developed in order to provide equal testing stress condition over the printed circuit board and calculate maximal acceptable load for nondestructive bending tests.

Theoretical model for planar location has been developed for defect location in printed circuit boards. The application of developed method in acoustically transparent medium indicated that located area of the defect makes about 1 % of the total PCB area, what provides accuracy 2-4 time higher than that by the regular surface location.

Method for nondestructive strength diagnostics of solder joints on printed circuit boards based on pure bending cycling tests with method of acoustic emission has been developed.

References

[1] State Industrial Standard GOST 53251-2014. Printed Circuit Boards. Classification of Defects, 2014.
[2] State Industrial Standard GOST 18353-79. Nondestructive Tests. Types Classification, 1980.
[3] **Royzman V. P., Kovtun I. I., Goroshko A. V.** Location of defects by acoustic emission method. Visnyk of Technological University of Podillia, Vol. 1, Issue 2002, 1, p. 195-200.
[4] **Kovtun I., Boiko J., Petrashchuk S., Baurienė G., Pilkauskas K.** Effects of the strain transmission from the main board to the installed electronic components. Mechanika, Vol. 22, Issue 6, 2016, p. 489-494.
[5] **Kühl Reiner W.** Mechanical stress and deformation of SMT components during temperature cycling and PCB bending. Soldering and Surface Mount Technology, Vol. 11, Issue 2, 1999, p. 35-41.
[6] **Pisarenko G. S., Kvitka O. L., Umanski E. S.** Strength of Materials, 2nd Edition. High School, Kyiv, 2004, p. 655.
[7] OST4 GO.054.089. Electronic Units and Blocks. Soldering Contact Joints. Sample Technological Processes, 1982.
[8] **Rao A. K.** Acoustic emission and signal analysis. Defence Science Journal, Vol. 40, 1990, p. 55-70.
[9] **Kuznetsov V. A., Dolgov V. A., Konevskikh V. M.** Measurements in Electronics: Handbook. Energoatomisdat, Moscow, 1987, p. 512.
[10] **Royzman V. P., Kovtun I. I., Goroshko A. V., Prokhorenko S. V.** Device for Coordinates Determination of Acoustic Emission Source, Patent 41138, 2001.
[11] **Royzman V. P., Kovtun I. I., Goroshko A. V., Prokhorenko S. V.** Method for Defect Location Using Acoustic Emission Method. Patent 43125, 2002.

Vilen Royzman received Doctoral degree in Machine Engineering Institute of Science Academy of USSR, Moscow, Russia, in 1979. In 1980 he received title of Professor. Now he works at Khmelnytsky National University as Head of Department of Telecommunication and Radio Engineering. His current research interests include vibrations, rotor balancing, inverse problems and strength in electronics.

Igor Kovtun received Ph.D. degree in Khmelnytsky National University, Khmelnytsky, Ukraine, in 1998. In 2000 he received title of Associate Professor. Now he works at Khmelnytsky National University as Head of Art and Technical Graphics Department. His current research interests include strength in electronics, nondestructive control, dynamics and fault diagnostics.

Andriy Voznyak obtained Master's degree in restoration and enhancement of wear resistance of parts and constructions specialty in Khmelnytsky National University, Khmelnytsky, Ukraine, in 2014. Now he works at Khmelnytsky National University as Research Fellow of Science and Research Department. His current research interests include strength in electronics, nondestructive control, dynamics and fault diagnostics.

5.2. Modified method of spectral analysis of the reflection signal for damage detection systems in power lines

Kostyantyn Horiaschenko[1], Victor Stetcuk[2]
Khmelnitsky National University, Khmelnitsky, Ukraine
E-mail: [1]*kostyakst@ukr.net*, [2]*sv_rt@i.ua*

Abstract. The work is devoted to the aspects of using phase methods for measuring distances to faults in a power line. The existing phase methods are shown and discussed. It is established that spectral leakage is one of the problems of spectral analysis. An algorithm for spectral analysis based on a change in the width of the analysis window is proposed. It is shown that the proposed method provides an increase in the accuracy of determining the amplitudes of the total signal components.

Keywords: power line, phase angle shift, spectral analysis, spectral leakage.

1. Introduction

1.1. The problem of measuring of parameters of power lines

Controlling of power lines state is a well-known problem. Usually measuring of parameters of such lines requires two categories of actions [12]:

1) The first category is a global analysis. Global analysis consists in determination of the state of the whole power line. As a result, we have information about state of whole line. In compare with previously measured data, detailed measuring can be required.

2) The second category is a local analysis. Analysis consists in measuring of parameters from point to point. Many methods used to do such measuring. However, each of them has advantages and disadvantages.

The presented categories connected to each other, but they do not interchangeable. The methods in the first category put on an aim verification of readiness to work or accordance of the already on-the-road system to the further use. Therefore, we have information about state of all power line. The methods in the second category used not only with the aim of measuring of parameters of power lines. A principal difference is ability for determination of current state of each part of power line. As a result, we can control local damages at any distance in line.

Measuring of parameters of the power line or system of power lines is a difficult process which require the use of one or a few simultaneously technologies.

A lot modern methodologies used for implementation of measuring [3, 6, 12]:

1. Time Domain Reflectometry, TDR.
2. Partial Discharge, PD (working frequencies varies from 50/60 Hz down-to 0.02 Hz (VLF)).
3. tgδ (tanδ), analysis of the dielectric penetrating on different frequencies.
4. Measuring of recovery Voltage.
5. DC Leakage Current.
6. Application of combinations of methods.

Many from these measuring methods already used in measuring devices, others are not yet accepted [10]. The use of various methods of measuring in power lines in the USA [12] are shown on Fig. 1.

For practical use only VLF, tgδ and TDR accepted. Other methods are on the stage of research or do not have commercial use. We have two fundamental groups:

a) The destructive measuring methods based on use of over-voltages. Such methods not only detect defects, they speed-up destruction of power lines.

b) The non-destructive measuring methods based on use of low and nominal voltages. Those

methods can be used without interrupting normal work of power lines.

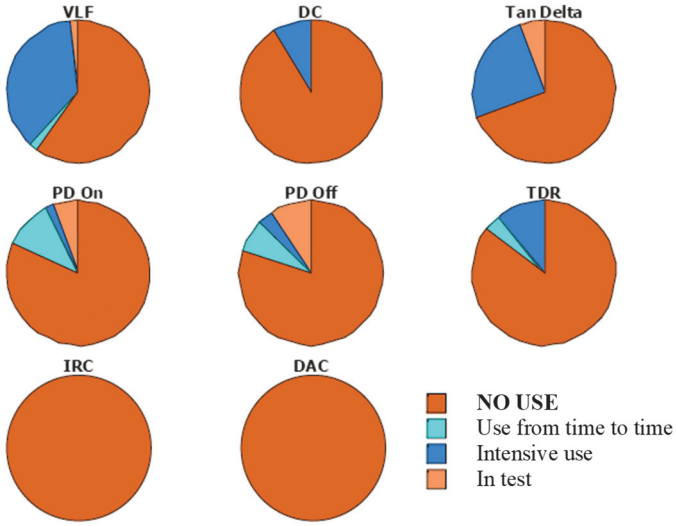

Fig. 1. The methods of measuring: VLF – very low frequency, DC – direct current, Tan Delta (tgδ) – measuring of dielectric losses, PD On and PD – partial discharge methods, TDR – time domain reflectometry, IRC – Isothermal Relaxation Current, DAC – Damped AC

1.2. Known phase measuring methods for distance measuring

1.2.1. Classic phase measuring method

Phase measuring methods based on measuring of phase shift [19-21] between applied test signal $\omega_0 = U_{m1}\cos\varphi_1$ and returned signal from reflection:

$$\omega_{01} = U_{m1}\cos(\Omega_m t + \varphi_{01}), \tag{1}$$

where U_{m1} – an amplitude of test signal; Ω_m – a frequency of scale frequency, in simplest case $\Omega_m = \omega_0$; φ_{01} – a phase angle shift on frequency ω_0 for the same object in line.

The returned signal looks like:

$$s_2(t) = U_{m2}\cos\varphi_2 = U_{m2}\cos\left(\Omega_m(t - t_R) + \varphi_{01} + \varphi_{ap} + \varphi_{\text{ret}}\right) \tag{2}$$

where U_{m2} – amplitude of returned signal; φ_{01} – an initial angle; φ_{ap} – a angle shift in the apparatus; φ_{ret} – a phase angle shift at the reflection.

Distance to reflection in air determined as [19, 20, 22]:

$$R = \frac{c\left(\varphi_\Delta + \varphi_{ap} + \varphi_{ret}\right)}{2\Omega_m}, \quad R = \frac{c\left(\varphi_\Delta + \varphi_{ap} + \varphi_{ret}\right)}{2\omega_0}, \tag{3}$$

where c – speed of signal in air.

For a physical environment with speed of distribution υ distance will be determined as:

$$R = \frac{\upsilon\left(\varphi_\Delta + \varphi_{ap} + \varphi_{ret}\right)}{2\omega_0}. \tag{4}$$

A value of phase angle shift φ_{ap} can be eliminated by calibration. The phase angle shift at the

reflection of signal φ_{ret} strongly influence with result – distance. That is why for measuring distance by phase angle shift method value of φ_{ret} is only ±180° (Fig. 2).

Use of classical phase measuring method based on the following principles in case of two or more reflections in any electrical line [18]:

- All signals pass through environments without fading;
- Speeds of wave distribution in all environments are identical;
- A signal is reflected in accordance with to the reflection coefficient of this object;
- Size of damage as small as possible, a zero-size of damage used as a rule;
- Signals passes power line pass without distortions.

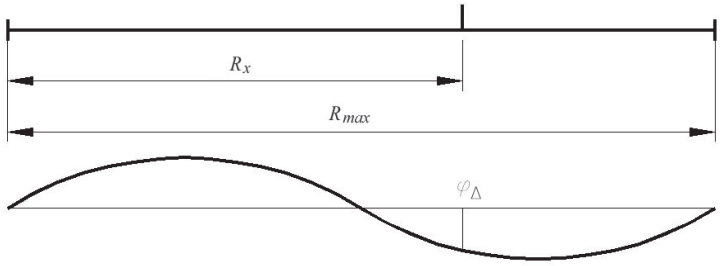

Fig. 2. Phase angle shift method

Simple case of two objects is shown on Fig. 3. Objects are located at distances l_1 and l_2 from the start of line. Accord to shown principles, a signal from the first object will be reflected with a phase angle shift φ_1. A phase angle shift can be expected after a formula:

$$\varphi_1 = 2 \cdot 2\pi \frac{l_1}{L_{\max}}. \tag{5}$$

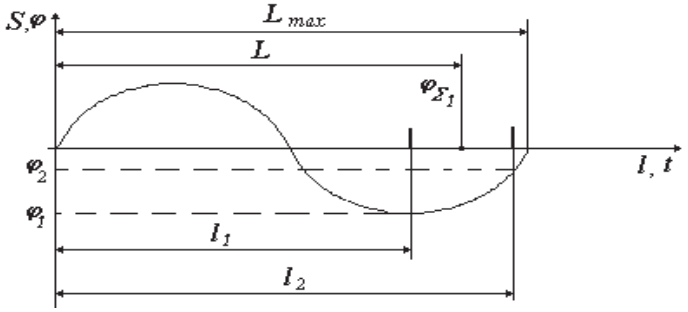

Fig. 3. Phase angle sift in case of existence of two objects

For the second object a phase angle shift φ_2 will be:

$$\varphi_2 = 2 \cdot 2\pi \frac{l_2}{L_{max}}. \tag{6}$$

Amplitudes of signals from every object depend on reflection coefficients Γ_1, Γ_2 and amplitudes of input signal a. Thus, we have:

$$a_1 = \Gamma_1 a, \;\; a_2 = \Gamma_2 a. \tag{7}$$

All signals are harmonious with one frequency and different phase changes. Thus:

$$s_{refl\ \Sigma}(t) = a_1 \cos(\omega t + \varphi_1) + a_2 \cos(\omega t + \varphi_2). \tag{8}$$

In this case, from Eq. (10) with use of Eq. (4) we will receive signal like $s_{refl\Sigma}(t) = A_\Sigma \cos(\omega t + \varphi_\Sigma)$ – signal from imaginary one object. And this object not at distance l_1 or l_2. This expression shows the most problem of classic phase distance measuring method – no possibility to separate objects in the process of measuring.

Other problem we have is a case of vagueness of distance measuring when a wave-length λ less than length of line L. Distance:

$$l = \frac{\lambda(2\pi \cdot n + \varphi)}{2\pi},$$

where n is integer from 0 to$[L/\lambda]$.

For the measuring with higher accuracy used so-called multiscale method [16, 17]. This method based on forming of set of frequencies from the lowest frequency, wave-length of which will be greater than length of line which is tested.

Advantages of that method:

• High exactness of determination of change of phases allows to get high exactness of distance-finding to the damage;

• Using of low frequencies allows to simplify construction of measuring device and diminishes a sensitivity to the external factors;

• Measuring phase angle shift is possibly during long time which improves overall accuracy.

1.3. Modern phase angle shift measuring methods and devices

With grow of electronic devices with large memories and high speeds new methods of distance measuring were developed. Those methods are based on use of sine wave signals and measuring of frequency of beating, as functions of distances [4, 8, 14]. Unlike TDR, new methods belong to frequency dimension reflectometry (FDR).

There are three types of frequency dimension reflectometry that use for measuring distances to damages. To such methods belong:

1) Frequency Modulated Continuous Wave (FMCW) [5, 9, 15];
2) Phase Detection Frequency Domain Reflectometry (PD-FDR) [9, 15];
3) Standing Wave Reflectometry (SWR).

Let consider shortly each of them.

1.3.1. Frequency modulated continuous wave (FMCW)

FMCW change frequency of sine wave signal very quickly. As a result, frequency shift measured between test and reflection signals converted to a corresponding delay equivalent to distance to the object. However, this method did not find application in power lines through limitation on speed in which a signal can spread in a line. Insufficient accuracy in which the frequency shift can be determined [8] is also determined.

1.3.2. Phase detection frequency domain reflectometry (PD-FDR)

System of measuring of distance which is based on measuring of phase angle shift shown in Fig. 4 [5-7], measures a phase angle shift between entrance and initial signals.

A voltage-controlled generator (VCO) provides a sine wave signal which steps in a line through the signal divider with a separation weak by –10 dB signal of the so-called “copy” of test signal (first mixer), and returns back in a device through the second mixer.

A mixer mixes together two sine wave that gives a sum and difference of these two frequencies. After that, analogue signals transformed to digital ones for fast Fourier transformation. This is a first method offered the use of accumulation of measuring information and treatment of them in a

single informative block.

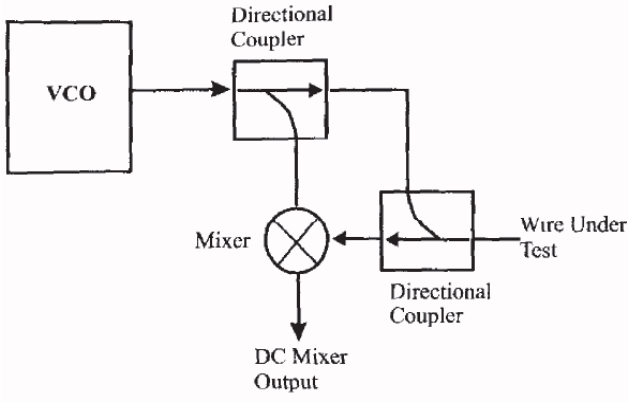

Fig. 4. Flow-chart of PD – FDR [7]

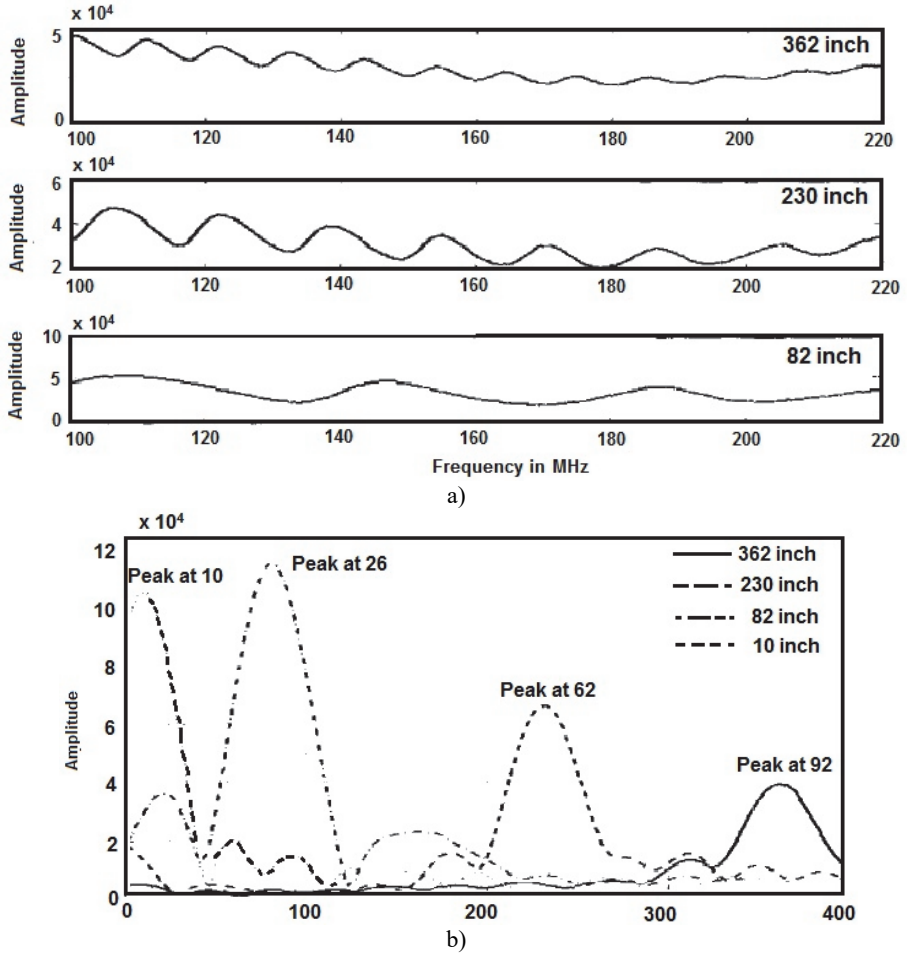

Fig. 5. Result of PD-FDR for the coaxial cable of RG-58 (50 ohm):
a) result on the exit of mixer; b) result of FFT [7]

FFT of the accumulated signal give a peak signals. Places of peaks in spectrum of FFT will

give distances to each of them. Distance can be found as [7]:

$$L = 2L_{\max}\left(\frac{Peak - Peak(0)}{N_{FFT} - 1}\right) = \frac{1}{2}\left(\frac{Peak - Peak(0)}{N_{FFT} - 1}\right)\left(\frac{N_F - 1}{f_2 - f_1}\right)\upsilon_p, \quad (9)$$

where $Peak$ – location of peak of delta function in FFT (integer value): υ_p – speed of distribution in a cable (m/s); f_1 – initial frequency of FDR (Hz); f_2 – eventual frequency of FDR (Hz); N_F – number of frequencies in FDR, usually unit from $Int\left(\frac{f_2 - f_1}{\Delta f}\right)$; Δf – size of step of frequency for FDR (Hz); $L_{\max}$ – maximal length, shown below; N_{FFT} – number of points in FFT (integer value, on the whole 1024, 2048, 4096 or 8192).

The fundamental problem of PD-FDR is very high count of points for FFT, low separation ability of objects and large range of frequencies. The typical set of answers of different lengths (on the example of wire as M27500-24SE2S23, [7]) is shown on Fig. 5.

PD-FDR has lower cost and uses simpler electronic base in compare with TDR. Components for PD-FDR could be integrated in a single chip. In addition, PD-FDR is able to work with re-reflections.

Like to the method of TDR of diminishing to distance to the object from the beginning of line requires minimisation of test signal frequency. But this is not possible to very low frequencies [2, 5, 13].

1.3.3. Standing wave reflectometry (SWR)

Standing Wave Reflectometry measure the size of standing wave, created by imposition of test and reflected signals from line. A sum of these signals is two sinewave signals (see Eq. (10)) which usually identical amplitude. However, the problem of SWR is a detection of signals with low level of reflection. Therefore, the method of SWR used in case of short circuit or break.

Advantages of SWF are exactness, similar to PD-FDR in case of short circuit or break, where test and reflected signals approximately the same size. The reflected wave will be partly less, depending on distance, but require frequencies in kHz for measure.

1.3.4. Mixed signal reflectometry (MSR)

Mixed signal reflectometry (Fig. 6) is similar to PD-FDR without direction couplers or to SWR, which measures the size of standing wave. Like PD-FDR, voltage-controlled oscillator (VCO) provides a sine wave signal which steps above the given size of step. Combination of test and reflected signals passes through attenuator, which prevent the overload of mixer.

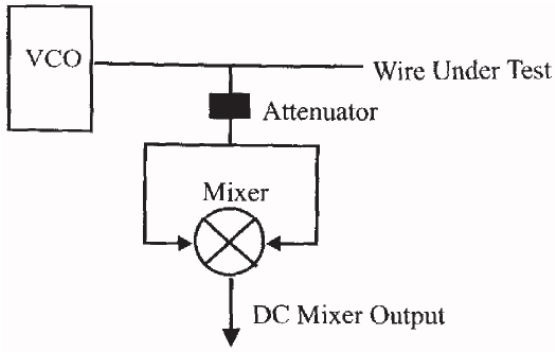

Fig. 6. Scheme diagram of MSR [7]

The method of MSR is more exact, than SWR for small reflections. However, this advantage

does not have practical application, because it does not allow analysing very little anomalies. MSR is less expensive and less cost than PD-FDR. For the lines with interconnections, reflected signal of MSR includes reflections plus their sums and differences, which does the answer more difficult for a calculation than PD-FDR. MSR have the same limitation on the use on live wires identically to PD-FDR.

1.4. Phase method for measuring distances of simultaneous objects in power line

Classic phase measuring method based on determination of phase angle shift φ between test input signal and reflection of the known frequency f_s [19, 20, 22].

A vector diagram (Fig. 7) serves for explanation of problem of phase methods. Diagram shows forming of summary signal $U_\Sigma \cos\varphi_\Sigma$ [18]. An analogical diagram can be created for 3rd, 4th or other amount of damages. A result is an signal of reflection with the corresponding summary phase angle shift φ_Σ.

Multiscale method of measuring of distances to the damages leading and optical to the flow line it is known from works of such scientists as Maevsky S. M., Bajenov V. H., Baturevich E. K. The multifrequency phase measuring method is used practically for measuring.

On Fig. 8 presented reflecting in the case of two objects with zero-size damages. Distances to the damages accordingly $l_1 = 1000$ m, $l_2 = 2000$ m. Amplitude of the first reflection has a level a 1.0 units (vector A), second is 0.5 units (vector B).

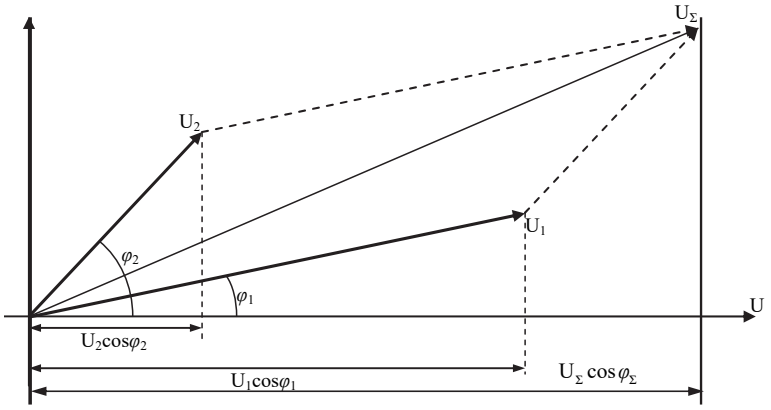

Fig. 7. Forming of reflection signal. Here: U_1, U_2 are amplitudes of reflections from 1st and 2nd objects, φ_1, φ_2 are corners of change of phase; $U_1\cos\varphi_1$, $U_2\cos\varphi_2$ are corresponding reflections; U_Σ it is summary amplitude and $U_\Sigma\cos\varphi_\Sigma$ is a summary signal

As shown on Fig. 8, at the change of test signal frequency in 2, 4 or 20 times, the angle shift changes gradually too. A change of the phase angle shift is proportional to frequency change.

Will pay attention to dynamics of change of vector A and vector B separately (Table 1). Especially interesting situation for understanding processes with frequencies 12ω and 20ω. On these frequencies is observed transition through 2π and 4π.

As seen from the Table 1, the increase of frequency and phase angle shift characterize every reflection. Let assume that measuring device consist of the generator of variable frequency $\omega(t_i)$. $\omega(t_i)$ is a frequency of signal during time t_i, $t_i \in [t_{i1}, t_{i2}]$. During time t_i from t_{i1} to t_{i2} frequency $\omega(t_i)$ held unchanged and duration of interval $[t_{i1}, t_{i2}]$ is enough for stabilizing of transients in a power line. As a result, we have change of phase angle shift for i reflection:

$$d\varphi_i = \varphi_i\big(\omega(t_2)\big) - \varphi_i\big(\omega(t_1)\big),$$

what takes place at the change of test frequency $d\omega_i = \omega(t_2) - \omega(t_1)$.

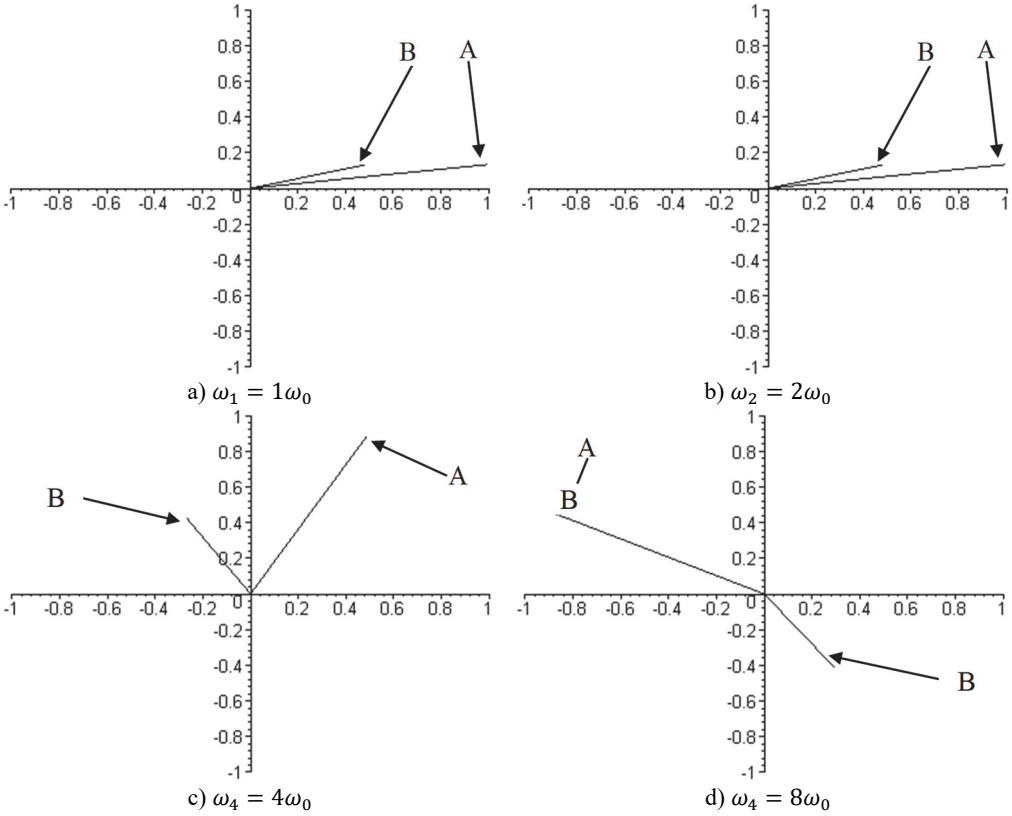

Fig. 8. To explain process of phase angle shift changes for two reflections on distances l_1, l_2 at the increases of frequency ω, $\omega_0 = 4 \cdot 10^3$ Hz

Table 1. Values of phase shift angles

Frequency, ω	φ_1, grad	φ_2, grad
1ω	19.2	38.4
2ω	38.4	76.8
4ω	76.8	153.6
8ω	153.6	307.2
12ω	230.4	460.8 (360+100.8)
20ω	384.0 (360+24.0)	768.0 (2×360+48)

Thus will enter a term "rotation of phase angle shift" $\Omega_{i,[\omega(t_1),\omega(t_2)]}$:

$$\Omega_{i,[\omega(t_1),\omega(t_2)]} = \frac{\varphi_i(\omega(t_2)) - \varphi_i(\omega(t_1))}{\omega(t_2) - \omega(t_1)} = \frac{d\varphi_i}{d\omega_{t_2 - t_1}}, \tag{10}$$

where t_1, t_2 are certain physical time domains at which a value of frequency of measuring signal is became.

A value of $\Omega_{i,[\omega(t_1),\omega(t_2)]}$ is a function of only frequencies and differences between the phase shift and frequencies.

In comparing with PD-FDR, value of $\Omega_{i,[\omega(t_1),\omega(t_2)]}$ is more prediction and give ability to work with low and high frequencies. It allows utilizing several intervals of frequencies in comparing

with PD-FDR where wide range of frequencies required.

Let assume phase angle shift for ith damage is determined from the known expression as:

$$\varphi_i = \frac{2\pi \cdot 2l_i}{\lambda},$$

or in more comfortable form circular frequency ω_j of test signal:

$$\varphi_i = \frac{2\pi \cdot 2l_i}{\upsilon} \cdot f_j = 2\frac{l_i}{\upsilon} \cdot \left(2\pi \cdot f_j\right) = 2\omega_j \frac{l_i}{\upsilon}, \tag{11}$$

where l_i – a distance to ith object which a reflection is from; υ – a speed of distribution of signal in an environment; ω_j – a jth frequency of testing signal.

In addition, expression what connect "rotation" $\Omega_{i,[\omega(t_1),\omega(t_2)]}$ of reflection vector with distance to the damage will be:

$$\Omega_i = \frac{\left(2\omega_{j+1}\frac{l_i}{\upsilon}\right) - \left(2\omega_j \frac{l_i}{\upsilon}\right)}{\omega_{j+1} - \omega_j} = 2\frac{l_i}{\upsilon} \cdot \frac{\omega_{j+1} - \omega_j}{\omega_{j+1} - \omega_j} = 2\frac{l_i}{\upsilon} \tag{12}$$

By limitation of frequencies from ω_{min} to ω_{max} the turn-down of phases will lay down:

$$\varphi_{i\,min} = 2\omega_{min}\frac{l_i}{\upsilon}, \quad \varphi_{i\,max} = 2\omega_{\max}\frac{l_i}{\upsilon}. \tag{13}$$

From (15) there is fundamental possibility not only to define frequency of reflections vectors rotation, and it is possible to define and amount of turns of vectors of phase angle shift for the ith reflection in this range:

$$N_{i\,turn} = \frac{\varphi_{i\,max} - \varphi_{i\,min}}{2\pi}, \tag{14}$$

or:

$$N_{i\,turn} = \frac{\frac{2l_i}{\upsilon}[\omega_{max} - \omega_{\min}]}{2\pi} = \frac{\frac{2l_i}{\upsilon}[2\pi f_{max} - 2\pi f_{min}]}{2\pi} = \frac{2\pi\frac{2l_i}{\upsilon}[f_{max} - f_{min}]}{2\pi} = \frac{2l_i}{\upsilon}[f_{max} - f_{min}]. \tag{15}$$

The analysis of the expression Eq. (14) will give an expression for recognition Eq. (15). As a result, we receive the following: value of Eq. (15) gave to us ability to work practically with any frequency range Eq. (15). The second feature of Eq. (15) is that $N_{i\,turn}$ will not be always an integer value only.

In addition, limitation of working range of frequencies is also equivalent to additional value of phase angle shift for each of signals. At $f_{min} = 0$, an initial phase angle is always $\varphi_i \to 0$. In common case of $f_{min} > 0$ we will also have $\varphi_i > 0$ (clearly, that except those cases, when $\varphi_i = 2\pi \cdot n$).

In real power cables, frequencies lower then 10-20 kHz does not allow to archive acceptable qualify of measuring due to variable parameters of power line on low frequencies.

For example, on Fig. 9 shown code in Wolfram Mathematica for modelling power line from 0.001 Hz to 600 kHz.

After that will be received figures of phase shift $\beta[\omega]$ (Fig. 10), real and imaging parts of wave

impedance $\dot{Z}_{imp}[\omega]$ (Fig. 11). Parameters of power line are stable for measuring only at high frequencies.

```
fL=0.5*10^-3
fR=20
fC=0.25*10^-6
fG=0.1*10^-6
fmin=0.001
fmax=600000
α[ω_]=Sqrt[1/2*((ω^2)*fL*fC-
fR*fG+Sqrt[(fR^2+(ω^2)*(fL^2))*(fG^2+(ω^2)*(fC^2))])]
```

$$\frac{\sqrt{-2.\times10^{-6}+1.25\times10^{-10}\,\omega^2+\sqrt{\left(1.\times10^{-14}+6.25\times10^{-14}\,\omega^2\right)\left(400+2.5\times10^{-7}\,\omega^2\right)}}}{\sqrt{2}}$$

```
β[ω_]=Sqrt[1/2*(fR*fG-
(ω^2)*fL*fC+Sqrt[(fR^2+(ω^2)*(fL^2))*(fG^2+(ω^2)*(fC^2))])]
```

$$\frac{\sqrt{2.\times10^{-6}-1.25\times10^{-10}\,\omega^2+\sqrt{\left(1.\times10^{-14}+6.25\times10^{-14}\,\omega^2\right)\left(400+2.5\times10^{-7}\,\omega^2\right)}}}{\sqrt{2}}$$

```
Z[ω_]=Sqrt[(fR+I*ω*fL)/(fG+I*ω*fC)]
```

$$\sqrt{\frac{20+(0.+0.0005\,i)\,\omega}{1.\times10^{-7}+(0.+2.5\times10^{-7}\,i)\,\omega}}$$

```
γ[ω_]=β[ω]+I*α[ω]
```

$$\frac{\sqrt{2.\times10^{-6}-1.25\times10^{-10}\,\omega^2+\sqrt{\left(1.\times10^{-14}+6.25\times10^{-14}\,\omega^2\right)\left(400+2.5\times10^{-7}\,\omega^2\right)}}}{\sqrt{2}}+$$

$$i\,\frac{\sqrt{-2.\times10^{-6}+1.25\times10^{-10}\,\omega^2+\sqrt{\left(1.\times10^{-14}+6.25\times10^{-14}\,\omega^2\right)\left(400+2.5\times10^{-7}\,\omega^2\right)}}}{\sqrt{2}}$$

```
Plot[α[w],{w,fmin,fmax},PlotLegends→"Expressions"]
Plot[β[w], {w, fmin, fmax}, PlotLegends →"Expressions "]
Plot[{Re[Z[w]], Im[Z[w]]}, {w, fmin, fmax}, PlotLegends →"Expressions "]
```

Fig. 9. Code for modelling power line from 0.001 Hz to 600 kHz in Wolfram Mathematica

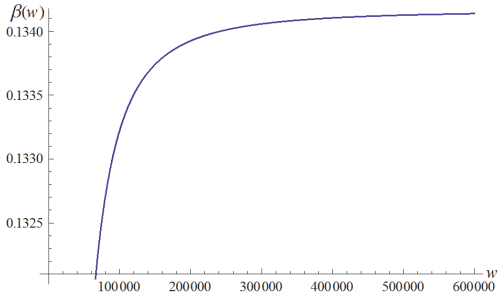

Fig. 10. Phase shift $\beta[\omega]$

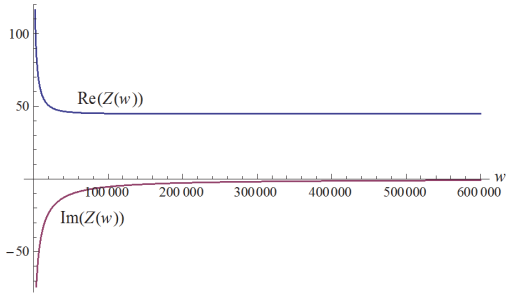

Fig. 11. real and imaging parts of wave impedance $\dot{Z}_{imp}[\omega]$

2. Signal modelling

On Fig. 12 it is shown distribution of the reflected signals $0.5\cos(6\varphi) + 0.7\cos(8\varphi) + 0.9\cos(10\varphi)$ for the range $\varphi = 0.2\pi$. That signal for modelling power line with 3 objects in it with distance 6:8:10 respectively. As were shown on Fig. 5(a) high frequency belong to far object. Limitation in a frequency range taken from Fig. 10 and Fig. 11. As

evidently, the initial phase of signals in allowed zone are different on such condition.

A spectral analysis of reflection signal with use of Fourier transformation with variable window size.

As were specified early, signal in phase measuring methods is sum of harmonics signals of the same frequency but with different phase angle shifts (see (10)). Due to different values of φ_i values of $\Omega_{i,[\omega(t_1),\omega(t_2)]}$ are different too. So, the object of analysis is a set of $\Omega_{i,[\omega(t_1),\omega(t_2)]}$.

Among the existent methods used for signal analysis, the most used methods are [1, 22, 23]:

- Fourier transformation;
- Wavelet analysis;
- Other methods of analysis.

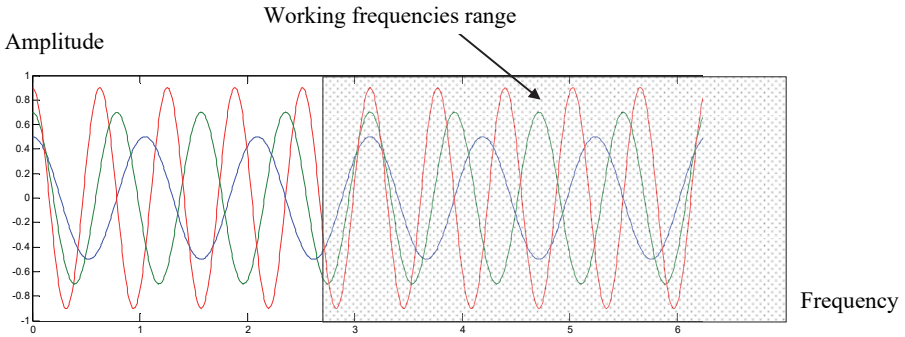

Fig. 12. Distribution of projections of vectors from the signals of reflections (signal $0.5\cos(6\varphi) + 0.7\cos(8\varphi) + 0.9\cos(10\varphi)$)

Fourier transformation is the well-known basic instrument of signals analysis in a frequency area. It is known that the periodic signals of kind $x(t) = x(t + mT_O)$ appear as a row of a sum of harmonic constituents.

In practice of spectral analysis of the real signals does not operate a continuous signal $x(t)$ and only by the eventual sequence of their selections $x(n)$. For this reason, in the technique of digital analysis of signals, discrete Fourier transformation is used.

The one of the main problem of FFT is analysing periodical signal limited in time. There are signals with period match analysis window size. And others are not equal to analysis window. Thus, if a periodical signal does not match with FFT window size additional components appear in a spectrum. This phenomenon named spectrum leakage. Spectrum leakage is possible to illustrate with the calculation of spectrum of discrete harmonic signal (Fig. 13) on an example. Discrete signal contains 16 points of harmonic signal with own period even to a 4 point (Fig. 13(a)) the periodically continued signal is periodic to FFT window.

If signal does not periodic to FFT window spectrum leakage will be observed (Fig. 13(b)). Spectrum of signal consists of additional harmonics. For PD-FDR or any equivalent method this mean additional objects in line.

To determine the methods for controlling the spread of the spectrum of the input signal, it is necessary to establish the factors that lead to the occurrence of this phenomenon.

Understanding the causes of the phenomenon in this case will allow taking a number of measures to eliminate the spread of the spectrum.

As were shown above, the phenomenon of the spectrum leakage is the appearance of additional harmonics in the spectrum. Moreover, these additional harmonics complicate the process of identifying harmonics from the real components of the signal. That is, there is a process of "masking" the signals. In order to deal with the spectrum leakage in the practice of digital analysis, it is known that window functions are used, but in this case, they do not give us the result we need because they reduce the phenomenon associated with the non-periodicity of the signal for analysis.

Window functions are used to reduce signal at beginning and ending of FFT window. For

example, Fig. 13 show use of Hann window function and result spectrum.

Given the complexity of the introduction of wavelet analysis and the need to create application software that would allow simple mathematical transformations, it would be able to transfer to 32-bit or 8-bit computing environment of small and medium computing power, proposed the creation of an algorithm for spectral analysis on based on the modified Fourier transform algorithm. Software implementations of the Fourier transformation are known for a large number of hardware and software environments.

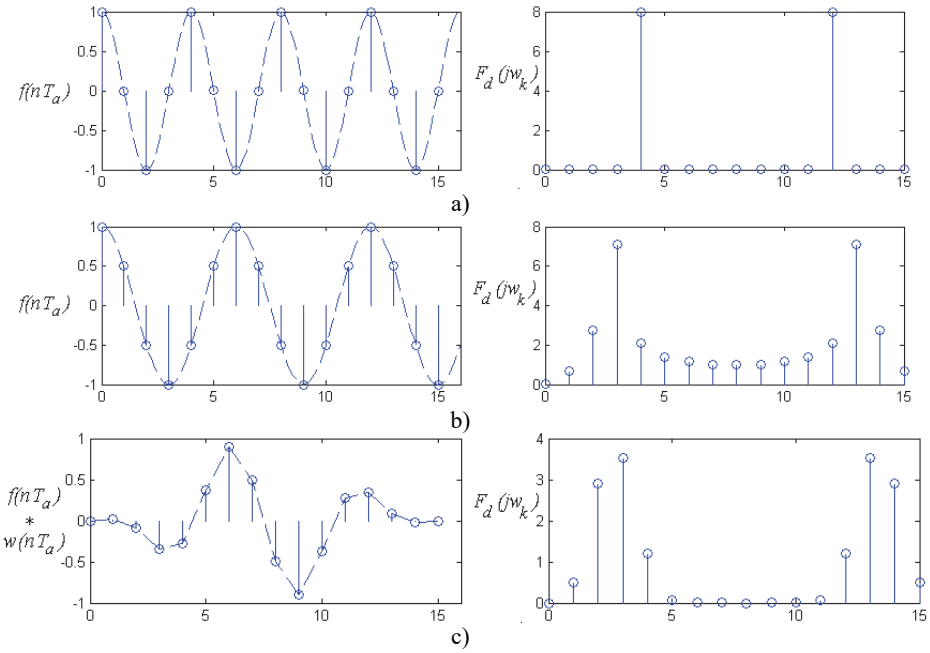

Fig. 13. FFT for periodical signal: a) unperiodical signal and spectrum leakage, b) reducing spectrum leakage with Hann window function

2.1. A flow-chart of spectral analysis algorithm

However, existing implementations does not allow detect signals with such incomplete period, since according to the FFT, the total signal represents a series of whole-periodic functions. Thus, if we change the number of points for FFT, it is quite clear that a signal with a non-integer period can transform into a signal with an integer number of periods, at the same time. But at the same time signals with integer number of periods will become signals with non-integer periods.

As a result of this, it is suggested to produce multiple analyses of the same signal by FFT. However, every next time of analysis the same signal point for FFT will be reduced. Since our signal represents a sum of harmonic signals, changing the window width will be in the coincidence of the whole number of periods. Accordingly, such signals in the output of FFT will have the highest amplitudes at a certain value of the window width. Consequently, the gradual decrease in the width of the window will lead to the discovery of various spectral components in the total signal.

Since there will be a rise and fall in the spectrograph, then it is proposed to highlight the largest and smallest values for each spectrogram in a single array. The aim of this is to determine the harmonics that have reached the highest value in the process of spectral analysis of our signal.

The algorithm for determining the spectral components of the total signal by manipulating the width of the window FFT is as follows:

1) Measuring of the input signal with the definition of N points.

2) A FFT cycle is performed. Result stored in arrays of maximal and minimal values.

3) Determine the spectral components with the greatest and smallest amplitudes. The result is remembered by adding to the result to the results of the previous cycles of the FFT.

4) Reduce the width of the FFT window by dropping one point from the end.

5) If the number of readings is greater than the minimum value of N_{min}, go to paragraph 2.

Conditionally, the flow-chart of algorithm of spectral analysis of signal with the change of width of window is shown on Fig. 14.

Software was created in the MatLab using the proposed algorithm.

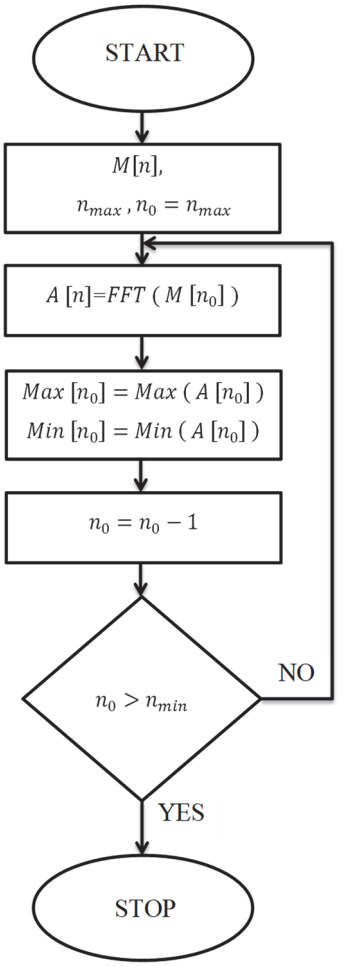

Fig. 14. Flow-chart of algorithm of spectral analysis with the change of width of window. Here $M[n]$ is an array of input data from measuring; n_{max} it is a number of the last element in an array $M[n]$; FFT it is a function of transformation of Fourier; $A[n]$ – the array of accordions is got on the ith step of transformation; $Max[n_o]$ and $Min[n_o]$ are arrays of most and the least amplitudes of accordions

2.2. Result of proposed algorithm

Consider the work of the proposed algorithm for spectral analysis of the signal with the change in the width of the FFT window. A signal is taken as a test signal (Fig. 15(a)) $-20\cos(64t + 0.7\pi) - 32\cos(74.3t + 1.2\pi) + 49\cos(106.2t + 3.2\pi)$.

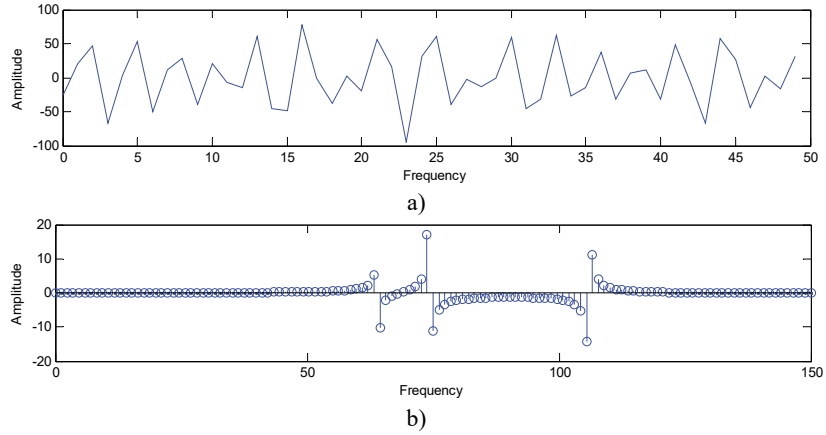

Fig. 15. a) Signal, b) spectral transformation for the signal of kind
$S(t) = -20\cos(64t + 0.7\pi) - 32\cos(74.3t + 1.2\pi) + 49\cos(106.2t + 3.2\pi)$

Fig. 16 shows the dynamics of changes of spectral components at the terms of FFT window width changed. It stipulates the necessity of setting of norms of the got result for a coercion to the only dimension to the landmark of frequency. At the same time, such setting of norms introduces error setting of norms, as spectral components, which have a whole number $N_{i,FFT}$ led to the corresponding rationed whole numbers:

$$N_{j,FFT} = round\left[\frac{Fs}{2}\cdot\frac{1}{NFFT'}\cdot k\right], \quad k = 1,\dots,NFFT', \quad NFFT' = \frac{NFFT}{2},\dots,NFFT,$$

where Fs is frequency of input signal discretization; $NFFT$ it is an amount of points of FFT.

For comfort of analysis, the result after normalization is shown on Fig. 17.

After FFT as shown on Fig. 15, amplitudes are only 12.1, 19.3, 16,1. After comparing result of FFT from Fig. 15 and from Fig. 17 can be noted following: the presence of three signals with amplitudes by modules 7.2, 13.1 and 17,4. Correlation between those amplitudes are closer to original ones in test signal.

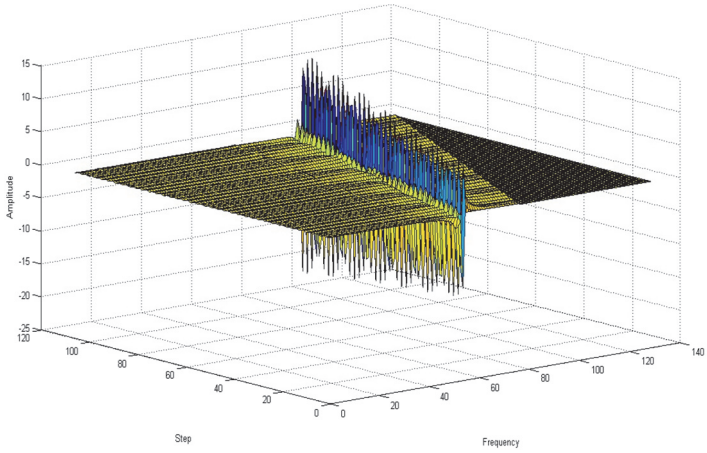

Fig. 16. Result in a 3-dimension view

Thus, offered method of determination of spectral component signals, which consist of harmonious signals with variables periods in compare to FFT window width allows to set both the

presence of spectral components and pick up correct amplitudes of these components. After FFT as shown on Fig. 15, amplitudes are only 12.1, 19.3, 16,1.

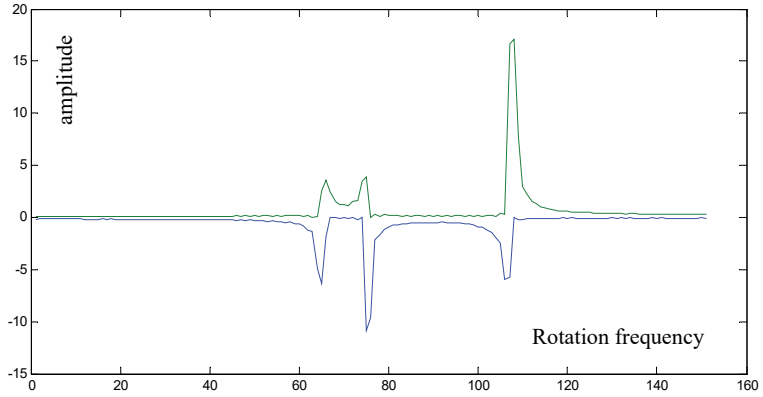

Fig. 17. Result of selection of spectral components by determination of maximal and minimum values of amplitudes of spectrums

3. Conclusions

There are a huge number of methods of spectral analysis, but they have properties that complicate their use in practice. Fast Fourier transform is a simple analysis method. However, the Fourier transform has errors in determining the frequencies and amplitudes of the components when the width of the analysis window and the period of the input signal are not identical. Spectral analysis based on wavelet analysis is a powerful tool, but complex and not sufficiently convenient for transfer to automated measuring systems.

The algorithm of the spectral analysis of the signal with the change in the width of the window is proposed. A simulation has been performed. Application of a variable width of a window allows reduce the influence of the spectrum leakage.

It is established that existing phase measuring methods have fundamental frequency constraints, especially at low frequencies below 100 kHz. Therefore, phase measuring methods have additional difficulties in practical application, since one of the key properties is considered to be the measurement at frequencies close to zero. At the same time, the frequency limitation is not principle for the presented phase-frequency method.

References

[1] **Amara Graps** An introduction to wavelets. IEEE Computational Science and Engineering, Vol. 2, Issue 2, 1995, p. 50-61.

[2] **Basava Santi B.** Detection and Location of Cable Faults Using Reflectometry Methods. M.S. Thesis, Ulah State University, 2004.

[3] **Filomena Andre D., Resener Mariana, Salim Rodrigo H., Bretas Arturo S.** Fault location for underground systems with capacitive current compensation. 16th PSCC, Glasgow, Scotland, 2008.

[4] **Chen C. S., Rocmcr L. E., Grumbach R. S.** Cable diagnostics for power cables. IEEE Annual Conference of Electrical Engineering Problems in Rubber and Plastic Industries, 1978.

[5] **Chung You Chung, et al.** Non-destructive fault location on aging aircraft wiring networks Part 1 – Cost-optimized solutions. IEEE AS and USNC/URSI National Radio Science Digest, Columbus, Ohio, 2003.

[6] **Hampton R. N., Perkel J., Hernandez J. C., Begovic M., Hans J., Riley R., Tyschenko P., Doherty F., Murray G., Hong L., Pearman M. G., Fletcher C. L., Linte G. C.** Experience of Withstand Testing of Cable Systems in the USA. CIGRE 2010, p. B1-303.

[7] **Chung You Chung, Turse Cynthia, Pruitt Jeremy** Application of phase detection frequency domain reflectometry for locating faults in an F-I8 flight control harness. IEEE Transactions on Electromagnetic Compatibility, Vol. 47, Issue 2, 2005, p. 127-114.

[8] **Furse C., Kamdar N.** An inexpensive distance measuring system for navigation of robotic vehicle. Microwave and Optical Technology Letters, Vol. 33, Issue 2, 2002, p. 84-87.

[9] **Furse Cynthia, Chung You Chung, Dangol Rakcsh, Nielsen Marc, Mabey Glen, Woodward Raymond** Frequency domain reflectometry for on board testing of aging aircraft wiring. IEEE Transactions on Electromagnetic Compatibility, 2003, p. 306-315.

[10] **Hartlein R. A., Hampton R. N., Perkel J.** Some considerations on the selection of optimum location, timing, and technique, for diagnostic tests. IEEE Power Engineering Society (PES) General Meeting Panel Session, Pittsburg, PA, 2008.

[11] **Oppenheim A. V.** Digital Signal Processing. Prentice-Hall, Englewood Cliffs, N.J., 1975.

[12] **Hartlein R., Hampton N., Hernández J. C., Perkel J.** Overview of Cable System Diagnostic Technologies and Application: Cable Diagnostic Focus Initiative Project (CDFI): 04-211/04-212/09-166. The National Electric Energy Testing Research and Applications Center (NEETRAC), Georgia, 2010, p. 323.

[13] **Schmidt Mark** Use of TDR for Cable Testing. M.S. Thesis, Utah State University, Logan, Utah, 2002.

[14] **Smith Paul** Spread Spectrum Lime, Domain Reflectometry. Ph.D. Dissertation, Utah Slate University, 2003.

[15] **Tsai P., Lo C., Chung Y. C., Furse C. M.** Mixed signal reflectometer for location of faults on aging wiring. IEEE Sensor Journal, Vol. 5, Issue 6, 2005, p. 1479-1482.

[16] **Abramov K. K.** Simulation and Calculation of Communication Cables on the Computer. Communication, Moscow, 1979, p. 79.

[17] **Gillmanov Eduard Akhnafovich**. Improvement of efficiency of cable transmission lines operation on the basis of their diagnostics by pulsed reflectometry. Ufa, 2009, p. 20.

[18] **Horiaschenko K. L.** Pulse-phase measurements for a line with two inhomogeneities. Measuring and computing engineering in technological processes. Khmelnytskyi. Vol. 1, 2003, p. 80-82.

[19] Cable Products. Terms and Definitions. GOST 15845-80, 1981, p. 18.

[20] **Glebovich G. V., Andriyanov A. V., Vvedensky Yu. V.** Investigation of Objects with Picosecond Pulses. Radio and Communications, Moscow, 1984, p. 256.

[21] **Lyubchik V. R.** Development of the phase method for measuring distances to two objects. Bulletin of the Technological University of Podillya, Vol. 2, 2004, p. 108-114.

[22] **Maevsky S. M., Bazhenov V. G., Baturevich E. K., Kuts Yu V.** Application of Methods of Phase Measurement for Precision Measurement of Distances. Higher School, Kiev, 1983, p. 84.

[23] **Otnes R., Enoxon L.** An Applied Analysis of Time Series: Basic Methods. Mir, Moscow, 1982, p. 430.

Kostyantyn Horiaschenko received Ph.D. degree in Kyiv National University of Technology and Design in 2005. Khmelnitsky National University. His current research interests include control and fault diagnosis in power lines.

Victor Stetcuk received Ph.D. degree in Khmelnitsky National University in 2012. Now he works at Khmelnitsky National University. His current research interests include telecommunications and power electronics.

5.3. Rank analysis in the problems of optimization of local power engineering

Serhii Denysiuk[1], Vasylenko Vira[2]
National Technical University of Ukraine, Igor Sikorsky Kyiv Polytechnic Institute, Kyiv, Ukraine
E-mail: [1]*spdens@ukr.net*, [2]*veravasylenko@gmail.com*

Abstract. The monograph considers the problems of efficient use of energy resources. The question of application of the technocenological approach for optimal management of energy consumption with the use of rank analysis, which includes procedures of interval estimation, parametric rationing, forecasting and standardization of consumption of resources is considered. The paper presents an algorithm for conducting rank analysis for forecasting power consumption and technocenose optimization. The practical example of technocenose optimization is presented and the rank-parametric distribution of technocenosis is shown on the parameter of electric consumption.

Keywords: energy efficiency, technocenosis, rank analysis, optimization of technocenosis.

1. Introduction

At present, energy consumption in the world has been increasing and fossil fuels comprise large proportion to the overall energy use. In addition to the concerned issue on future exhaustion of resources, global warming is also becoming a serious concern due to higher concentration of CO2 emissions in the air through the use of these resources. In regard to effective countermeasures against these global issues, the international community has actively made efforts on the promotion of energy conservation such as building the international framework in accordance with the Kyoto Protocol. On the other hand, countries still tend to focus on economic development rather than environmental countermeasures. Especially in developing countries, demand for energy has continuously increased due to the population growth and industrialization. It is expected that the world energy consumption will significantly increase, mainly in developing countries in the 21st century. It is necessary for both developed and developing countries to promote energy conservation in order to resolve the global issues for the future.

The basis of energy conservation in power systems is the planned implementation of a complex of technical and technological measures and optimization of energy consumption of their individual elements at the system level. The purpose of optimization is to streamline the energy consumption of the power system objects, to save energy resources received from the consumed primarily through organizational measures, as well as to create scientifically grounded assumptions for conducting targeted energy surveys, followed by the implementation of technical and technological measures for energy conservation [1].

Describing processes in the energy system, we use the following definitions:

Technical power system (TPS) – the summation of numbers of equipment and enterprises that interact with each other for the production, consumption or transformation, storage, transportation or processing of energy products.

Energy product – finished product, which is used mainly for the production of mechanical work.

Natural resources are used as inputs to TPS, in other words the summation of equipment and enterprises, the main outputs of which are products and services, but which also produce by-products and emissions. Natural resources of other energy sources such as solar radiation, tidal energy, geothermal energy, wind and heat are also used for direct conversion into mechanical, thermal or electrical energy.

Products that are outputs of the technical power system are inputs to other technical power systems or are used to provide services. At the end of their exploitation, they are reused within the technosphere or returned to the environment as emissions. Thus, inputs to the technosphere are

natural resources, and the outputs of services provided to society, emissions and operational influences [2, 3].

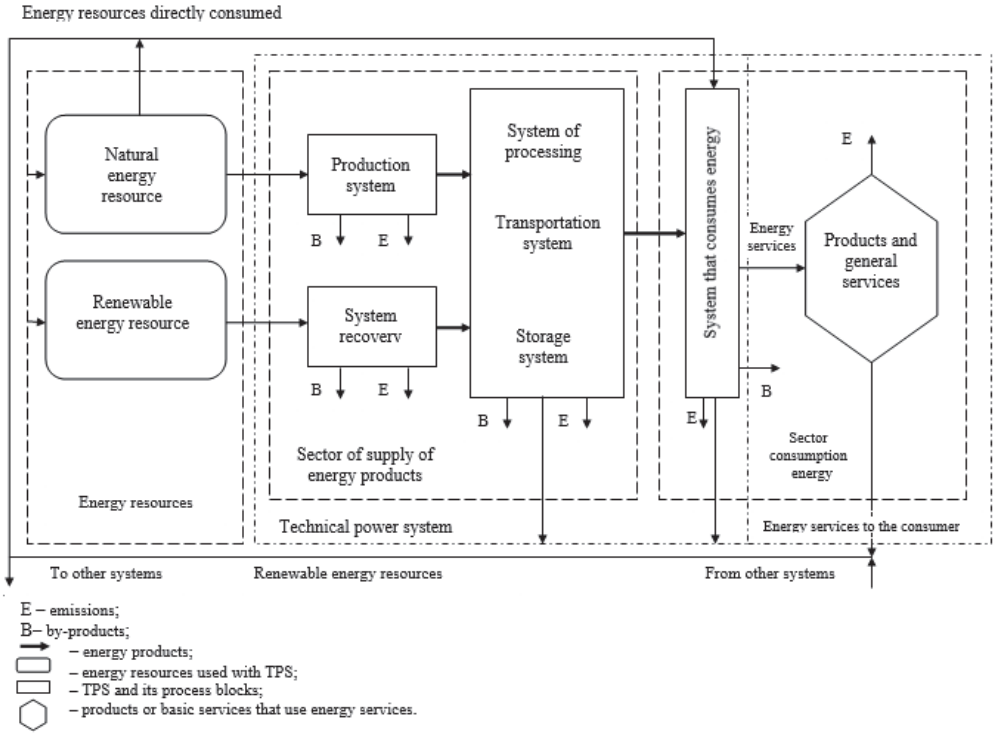

Fig. 1. The general model of the technical power system

2. The theoretical part

The general methodology of research and implementation in the field of energy conservation, according to the classification introduced in [4, 5], can be conditionally divided into three levels (Fig. 2):

1) The first level corresponds to activities aimed at specific technical and technological developments that contribute to reducing energy consumption (improvement of heat supply systems, replacement of outdated lighting devices, introduction of energy-efficient frequency controlled electric drives, modernization of internal equipment of buildings and structures, etc.).

2) At the second level, optimization of energy consumption of TPS as a whole is carried out. As a methodological basis at this level, a rank analysis based on the technocenological approach, Zipf mathematical statistics and the theory of hyperbolic infinitely divisive distributions is widely used. Given the conceptual and methodological differences that underlie research at the second level, it is considered to be systemic in relation to the level of research relating to specific technical and technological solutions in the field of energy conservation [6].

3) Strategic planning and forecasting of the TPS is carried out at the third level of activity (maneuvering of the maximum load, reduction of losses in the lines, effective control, etc.).

Real management of technocenosis is possible only in the conditions of correct understanding the object of management, as well as the introduction of correct methods for optimal management of this object.

Biological terminology is used to describe the technocenosis [7]:

• individual – an integral part of the cenosis – are personified TPS, which carry out unique activities, have an individual name, are taxpayers, independently distribute and consume resources;

• view – a group of elements, systematized by the nature of the activity, size;
• population – a group of individuals of the same species;
• caste – a group in which each species is represented by an equal number of individuals.

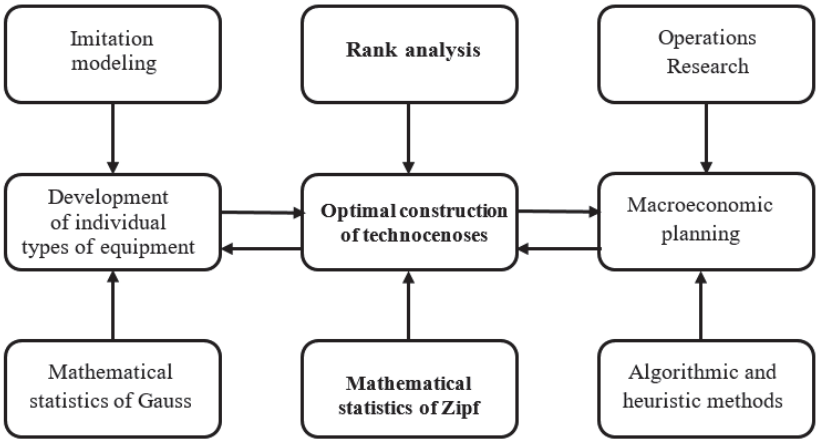

Fig. 2. Levels of research in the field of energy saving TPS

The main properties of technocenosis [8]:

1) The name and number of all available (winding transformer wire, fasteners, tools, instruments, etc.) cannot be listed. Each of the objects is discretely allocated as an individual, but at the same time it can be described by a variable parameter (costs, electricity consumption) from a continuous series of positive integers. The discreteness and finiteness of the elements forming the technocenose, as well as the continuity and possible change of the cenosis parameter in general, allow it to be formalized to describe it for evaluation of the past, management of the current state and forecast of development;

2) Uncertainty of the boundaries of electricity supply. They are not limited only to the master plan: own electric networks go beyond its limits, which feed on third-party consumers (the same thing - inside).

Speaking about the indicators that characterize the technocenosis (regardless of their verbal or formal representation), one should bear in mind:

1) The price cannot be adequately described by a system of indicators, any system is fuzzy and incomplete, an increase in the number of indicators and an increase in accuracy (reliability) does not approach to the selection of the technocenosis;

2) Two cenoses, described by one system of indicators, which coincide within the limits of accuracy adopted for this class, may differ in essence (characteristics, parameters, representations) [8].

Technocenosis has the following pronounced specific properties [4, 5, 9]:

1) interconnectedness – the individual objects of technocenose are statistically significantly related to a single system, but the type of connections in this case is special – these are so-called "weak" connections that are not reduced to the Newton's law, Ohm's law, Kirchhoff's law et al.;

2) "Gaussless" – statistical samples of the parameters of individuals (objects) have Zipf properties (the dependence of the mean and variance on the sample size is significant), that is, the law of large numbers is not executed, which consists in the fact that the average statistical value should converge on the probability of mathematical expectation. This suggests that, before starting to manage the infrastructure object, it is necessary to find out whether it is a technocenosis and, consequently, in general, whether it is possible to apply it to the technocenological methodology.

The main instrument of the technocenological approach in the study of complex technical systems is the rank analysis – the method of research of large technical systems (infrastructure),

which aims at their statistical analysis, as well as optimization, and uses the form of generic and rank distributions as the main criterion. Hyperbolic H-distributions are used to describe technocenosis.

Ranked distribution refers to the downward sequence of parameter values, arranged in such a way that each subsequent number is smaller than the previous one, and is brought into line with the rank (number in order, number of integers, arranged in ascending order) [3].

The structure of the cenosis is described by species distribution – the dependence of the number of species on the number of individuals in the form, ranked species distribution and rank distribution by parameter [7].

The mathematical apparatus of the cenological method is represented by three models of hyperbolic H-distribution (Fig. 3) [1, 8]:

1) Species:

$$\Omega(x) = \frac{W_0}{x^{1+\alpha}}, \tag{1}$$

where $x \in (1; \infty]$ – a continuous analogue of population numbers i, (i – always a discrete value, $i = [x]$); $a > 0$ – characteristic index; constant distribution $\gamma = 1 + a$; $W_0 = A \cdot S$, $W_1 = [W_0]$, where W_0 – the theoretical, not necessarily discrete value, and W_1 – actual (experimental) value of the first point; A – constant distribution, which is found from the conditions of valuation.

2) Ranked:

$$\Lambda(x) = \frac{B}{r^{\beta}}, \ \ \omega(r) = \frac{u_r}{U}, \ \ U = \sum_{r=1}^{S} u_r, \tag{2}$$

where u_r – the number of species of species (the population of the s_r species), which corresponds to rank r in the total number of individuals U. Rank of the species $s = 1,2, \dots, s_r, \dots, S$ – is a serial number (line number). $1 > B > 0, \beta > 0$ – constants of a rank-like H-distribution.

The species and rank distribution are used to study and manage the structure of installed equipment and equipment that is being repaired (electrical installations), that is, for discrete quantities. But the power supply system is characterized by continuous quantities (electricity consumption, heat consumption, capacity, cost, costs). In this case, the hyperbolic rank H-distribution by parameter [10] is used.

3) Ranked by parameter.

Let set of objects that form a certain integrity (all units of a single enterprise) and which correspond to cenological criteria. Each object is characterized by one or more parameters that are expressed numerically. After defining the parameter, you can arrange the set, placing all objects in order of decreasing the parameter, and obtain a hyperbolic rank H-distribution by parameter. The area under the curve of the rank H-distribution by parameter characterizes the energy consumption of the enterprise as a whole:

$$W(x) = \frac{W_1}{r^{\beta}}, \tag{3}$$

where r – the rank of the object; β – an indicator that determines the degree of steepness of the distribution curve; $W_1 = W_{max}(x)$ – the constant for which the maximum value of the energy consumption of the largest consumer is taken:

$$\beta = \log_r \frac{W_1}{W(x)}. \tag{4}$$

The ranking by parameter allows us to talk about the optimality, the effectiveness of the cenosa as a whole. Next it is necessary to investigate the structure of the cenosis. The best is the state of technocenosis, in which the parameter is within range $0.5 \leq \beta \leq 1.5$.

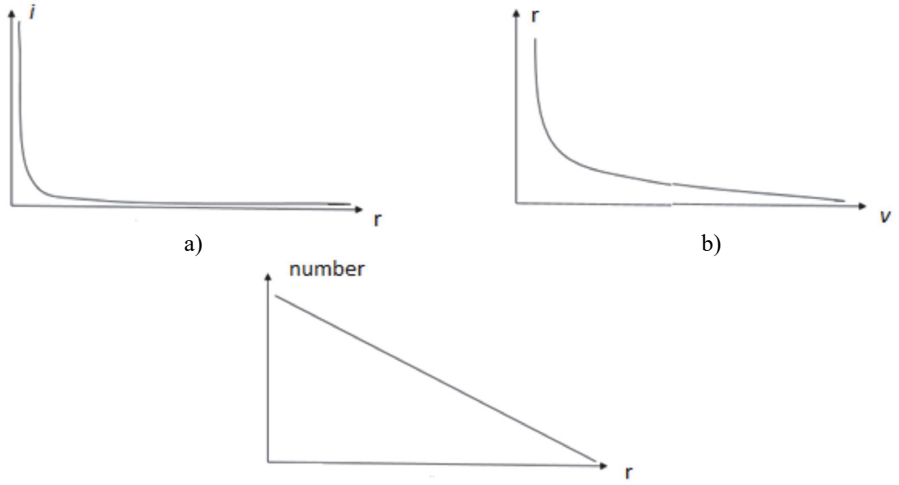

Fig. 3. Types of H-distributions: a) species distribution, b) rank distribution, c) ranked by parameter distribution

Removal of abnormal variations in the species distribution is based on the analysis of deviations from the approximating curve: upwards – indicate a lack of unification of species, and downward – on the contrary, excessive. Parametric optimization determines the detailed mechanism of the process of improving the structure of the cenosis on the basis of characteristic indicators.

The energy consumption of a separate TPS using a technosenological approach is considered not in isolation but correlated with other consumers, hierarchically systematized. Detection of the tendency of the electricity consumption of the power system of the region, analysis of the parameters of rank distributions creates the basis for optimizing the management of the electricity consumption of the infrastructure region, enabling more accurately predict the further development of the energy complex, assess its stability [11].

3. Materials and research results

Investigating cenosis as an integrity reduces to their systematic description of the hierarchical system of indicators (which is necessary for the identification of the cenosis) and to the structural cenological description. Consider the technocenosis of the TPS on the example of the specific energy consumption by technoenese individuals. This cenosis is limited in space – the total number includes many functionally isolated individuals, not connected with each other by strong ties. There is also a single infrastructure that includes a power supply system, as well as a control system for operation and operation.

Energy consumption of the power system is described by analytical dependence:

$$W(x) = \frac{W_1}{r^{\beta}} = \frac{501316.2}{r^{0.725}} \Rightarrow \beta = 0.725. \quad (5)$$

According to the above expression, one can determine some range of optimal states of the system and graphically display it as a certain band on the rank distribution graph (Fig. 4).

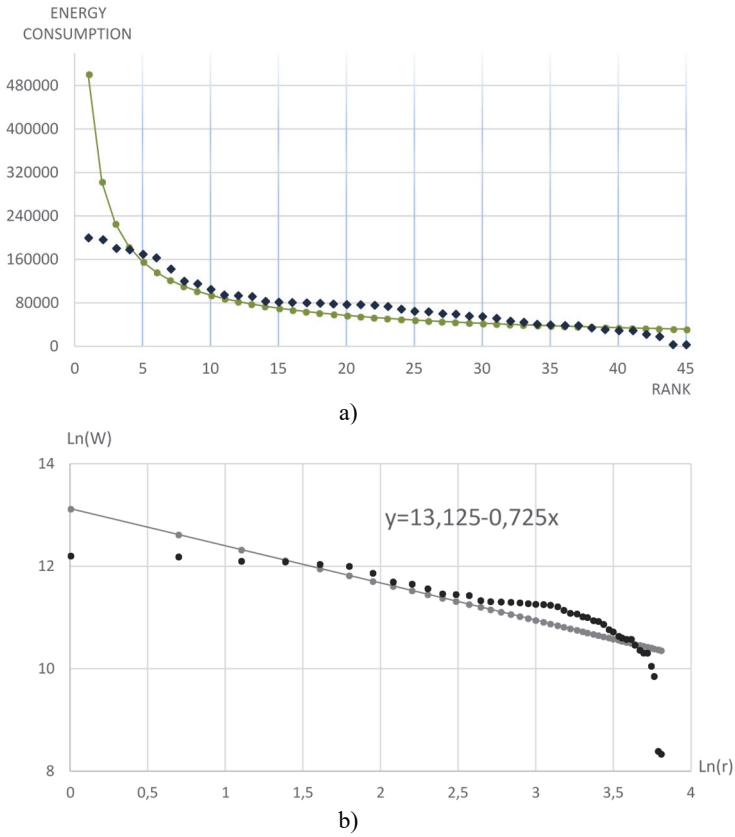

Fig. 4. The parametric distribution of the technocenosis of the TPS:
a) points – empirical data, b) solid line – approximation curve

Fig. 4 shows that the specific power consumption is not optimal enough and needs to be significantly improved. The parameter of the H-distribution is not within the range, the energy consumption curve is far removed from the optimal approximation curve, which indicates the inadequate performance of the system as a whole. Needed additional work with technocenose: nomenclature optimization; purposeful removal of abnormal individuals; parametric optimization; improvement of parameters of abnormal individuals, etc.

Rank analysis never ends with the approximation of the relevant technocenose distributions. It always follows optimization, because our main task is to determine the directions and criteria for improving the existing technocenose. The procedure for optimizing any cenosis is aimed at eliminating abnormal deviations in rank distribution. After the detection of anomalies in the graphical distribution of the tabulated distribution, individuals are identified, "responsible" for the anomaly, and identified the priority measures to eliminate them.

The algorithm for conducting rank analysis for optimizing technocenosis includes the following steps:

Step 1. Selection of the cenosis.

Selection of technocenosis is accompanied by its description. For this purpose, a special database is provided, which includes systematized and standardized, sufficiently complete and at the same time, without unnecessary details, information on the types and individuals of technocenosis.

Step 2. Setting of the shaping parameters.

Elements technocenose are allocated on the basis of the database. For each item there must be some documentation in the database. If we consider the case with TPS, then the database should

contain data on monthly energy consumption.

Step 3. Ranking – parametric description of the cenosis.

The first rank is assigned to an object with the highest energy consumption, further decreasing.

Step 4. Construction of the tabulated rank distribution and the graphical rank parametric distribution of the existing technocenosis.

Step 5. Calculation of the degree of steepness of the hyperbolic H-distribution curve. Approximation of distributions.

Step 6: Optimize the technocenosis.

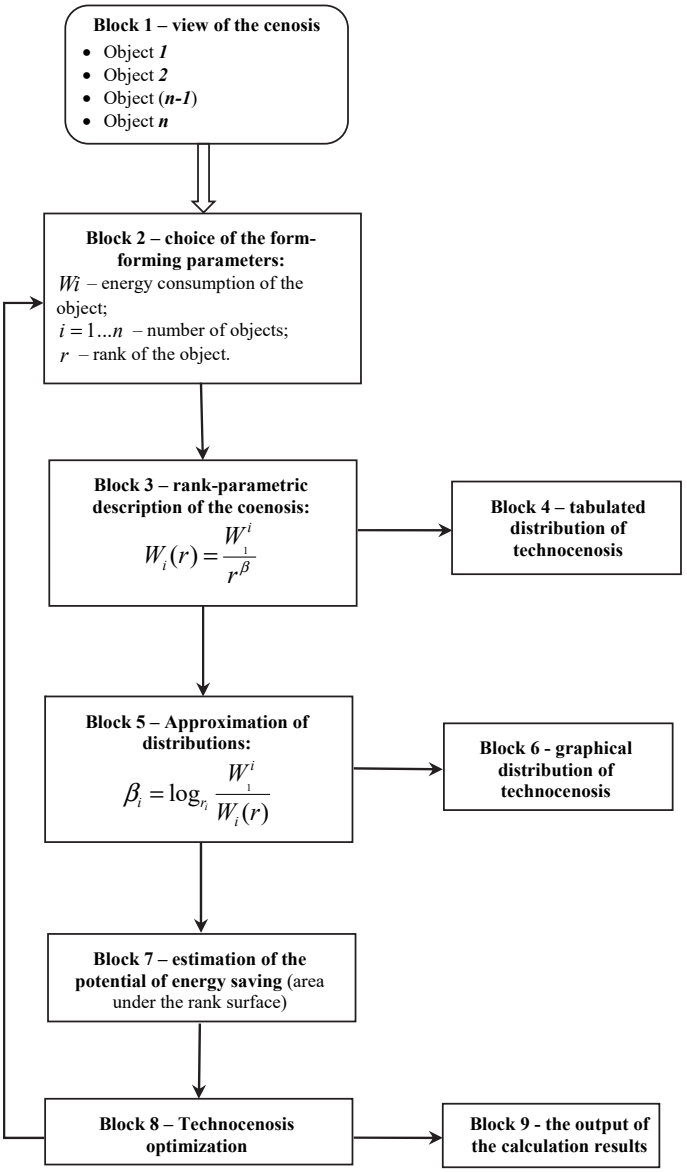

Fig. 5. Block-diagram of algorithm for conducting rank analysis for optimization of technocenosis

The best known technocenosis, which is a set of technical products, individuals who, on the one hand, their combined functional parameters provides performance tasks, and on the other –

has a maximum entropy, so the total energy resources embodied in technical products for their manufacturing, distributed evenly according to the populations types of equipment. Optimal improvement of the structure proposed tehnotsenozu carried out in two phases: the first phase to determine and optimize the basic types, and the second – to form a species diversity of species and parameters of technical products that meet the requirements dictated by law optimal construction technocenosis.

After this analysis it is possible to proceed with the forecasting of energy consumption on the basis of technocenological approach. The block diagram of the algorithm for conducting rank analysis for the optimization of technocenosis is presented in the Fig. 5.

4. Conclusions

The advantage of technocenological method and rank analysis is the optimal reflection of the process of functioning of technocenous objects in the future, taking into account possible changes in technology, infrastructure, and the use of resources. It is a disadvantage to note that the method based on a statistical model, as well as similar methods, with high accuracy calculates the value of short-term forecasting (according to studies, the exact forecast can be obtained for 1 to 2 years, after which the error is sharply increasing). Another disadvantage is the inability to implement criteria based on comparing power management options. These disadvantages can be eliminated. This requires the creation of a dynamic adaptive model that reflects the process of power consumption at a depth of 5 to 7 years or more.

This algorithm can be widely used for solving actual tasks of design, construction and operation of power systems, as well as for improving the quality and reliability of energy supply and implementation of energy saving measures, as well as new projects in the field of alternative energy.

References

[1] **Vasylenko V.** System efficiency of functioning of the power system with controlled loads. Power Engineering: Economics, Technology, Ecology. Vol. 1, 2015, p. 70-81.
[2] DSTU ISO 13600-2001 Power Engineering Systems. Basic Provisions, IDT, 1997.
[3] DSTU ISO 13601-2001. Power Engineering Systems. Structure for Analysis. Energy Supply and Consumption Sectors, IDT, 1998.
[4] **Gnatyuk V.** Technique, Technosphere, Energy Saving. Internet Moscow, 2012.
[5] **Gnatyuk V.** The Law of Optimal Construction of Technocenosis. Kaliningrad, 2014.
[6] **Prokopchik V.** Improvement the Quality of Power Supply and Efficiency of Electrical Equipment of Enterprises with Continuous Technological Processes. Gomel, 2002.
[7] **Kudrin B.** Power Supply for Industrial Enterprises: a Textbook for Students of Higher Educational Institutions. Moscow, 2005.
[8] **Kudrin B.** Tsenological bases of management by an electric economy of the consumer. Industrial Power, Vol. 9, 2015, p. 38-46.
[9] **Denisyuk S., Vasilenko V.** Optimal management of energy consumption of budget organizations and institutions as objects of technocenosis. Bulletin of the Kiev National University of Technology and Design, Series Technical Sciences, Vol. 5, Issue 114, 2017, p. 97-105.
[10] **Kosharnaya Y.** Use of methods of cenological and cluster analysis in energy audits of industrial enterprises. Proceedings of the 7th International Scientific and Practical Internet Conference on Energy and Resource Saving 21st Century, Orel, 2009.
[11] **Fedorova S., Tretyakov A.** Application of the technocenologycal approach to the analysis of power consumption and energy saving of enterprises of the Sverdlovsk Region. Bulletin of the South Ural State University, Vol. 16, 2012, p. 92-97.

Serhii Denysiuk Doctor of technical sciences, Professor, Director of the Institute of Energy Saving and Energy Management, National Technical University of Ukraine “Igor Sikorsky Kyiv Polytechnic Institute”, Kyiv, Ukraine. He is specialist in energy security and energy conservation.

Vira Vasylenko, Assistant of the Institute of Energy Saving and Energy Management, National Technical University of Ukraine “Igor Sikorsky Kyiv Polytechnic Institute”, Kyiv, Ukraine. Her current research interests include development of methods for increasing the efficiency of functioning of power supply systems with controlled loads through the implementation of the principles and laws of multi-agent management.

5.4. Principles of constructing invariant piezoresonance devices based on adaptive multifrequency systems with a predictive standard

Sergey Pidchenko[1], Alla Taranchuk[2]
Khmelnitsky National University, Khmelnitsky, Ukraine
E-mail: [1]*sergpchn@gmail.com*, [2]*allatr@ukr.net*

Abstract. The paper represents principles of developing invariant to disturbing factors piezoresonance units with controlled dynamics, which are assumed to be the adaptive control system with predictive reference model. There are formulated the objectives and criteria for terminal control and given results of research of piezoresonance three-frequency oscillation system dynamics on the base of developed mathematical model, containing generalized reduced differential equations, describing character of oscillations' amplitude, phases and voltages of auto-bias in excitation channels. On the base of modified method of simplexes the oscillation system parameter optimization is performed by minimum time criterion for three-frequency oscillation mode setup.

Keywords: quartz resonator, quartz crystal oscillator, multi-frequency oscillation system, frequency instability, destabilizing impact factors.

1. Introduction

The intensive progress in radio-electronics and measuring technology based on implementing digital and microprocessor technology increases the role of electronic components providing generation of high-stability clock frequency oscillations. The most common sources of reference oscillations are crystal oscillator (XO). Due to high stability of oscillation frequency, minor mass and size parameters and relatively low cost XOs are widely applied to systems for data transmission and radio communication, radio location and radio navigation, radio engineering measurements and telemetry, in computer technology and domestic radio devices. Also, piezoresonance (quartz) auto-generating sensors of physical parameters such as pressure, strain, acceleration, temperature, humidity and others are traditionally applied.

At the same time the further development in functionality of piezorasonance devices (PRD), quartz resonators (QR) and crystal oscillators, filters, piezoresonance transducers of physical parameters, which are undetectable parts of telecommunication and measuring systems, requires improving accuracy of their characteristics: stability of resonance frequency, bandwidth, parameters of generated oscillations and characteristics of physical measure transformations. Design, technological and functional methods (concerning compensation of destabilizing factors) are likely to meet difficult contradiction with modern requirements to microminiaturization, reliability, energy consumption, readiness time and costs.

One of the perspective ways along this line represent functional and algorithmic approaches to provide invariance of PRD to destabilizing factors. It refers to multi-frequency excitation mode of quartz resonator, what allows combining its basic function – frequency determining (stabilizing) function and additional (measuring) function to improve accuracy of the current QR condition identification.

However, proceeding to multi-frequency oscillation mode (MOM) of QR, because of competition of oscillations in excitation channels of QR, significantly complicates PRD dynamics, what may cause a loss of oscillation stability and essential increasing of transition processes in comparison with single-frequency mode. This fact significantly increases requirements to multi-frequency PRD parameter optimization to provide high sustainability and stability of oscillations and also decreasing its readiness time [1-6].

2. The multi-frequency functional-algorithmic methods to ensure invariant piezoresonance devices

It is known [7], that the absolute coordinates y_i of the invariance of influence x_j:

$$y_i(p) = \mathbf{\Phi}(p)x_j(p), \;\; i = \overline{1,n}, \;\; j = \overline{1,m}. \tag{1}$$

Necessary that:

$$\begin{aligned} &\Phi_{ij}(p) = \left(A_{ij_0}p^r + A_{ij_1}p^{r-1} + \cdots + A_{ij_r}\right)B_{ij}^{-1}(p^s, p^{s-1} \ldots p) \equiv 0, \\ &A_{ij_l} \equiv 0, \;\; \forall l = \overline{0,r}, \;\; r \le s. \end{aligned} \tag{2}$$

Having presented $A_{ij_l} = A_l^{(1)} + A_l^{(2)}$ (principle of dual channel), we get invariance condition Eq. (2) for passive differential (without identification) system:

$$A_l^{(1)} = -A_l^{(2)}, \tag{3}$$

which is satisfied by the selection of parameters of channel, for example, using two piezoresonance oscillation system (POS), which opposite in sign to the temperature coefficient of frequency. In the ideal case $y_i(t) \equiv g_i(t)$, that the real movement of system is corresponds exactly to the desired.

In practice, however $y_i(t) - g_i(t) = \varepsilon$, so further considered invariance PRD with accuracy to ε (the technical invariance). Beside this, because $j > 1$, is introduced the concept of multivariate.

In accordance with Eq. (1), PRD represented as multilateral multi-frequency transducer (MFT), which includes m destabilizing channels and n control channels.

It should be noted that the separation of all control channels to control and destabilizing it is a conditional. For example, the invariance of quartz oscillator requires fulfillment of Eq. (2) for all $m + n$ channels, but also the invariance of piezoresonance sensor the one physical quantity requires fulfillment of conditions for $m + n - 1$ channels. This choice allows the model with the same position is solve the problem of invariance of all existing PRD [7, 8].

3. Generalized formalized model of invariant PRD with current identification of impacts

Generalized invariant structure PRD with current identification impacts is developed on the basis of multiply system with combined management [5, 6], there are two regulation contours by the disturbance and the deflection (open-circuited and closed) can be synthesized separately, which is so important for solving the problem of invariance of piezoresonance devices. Given that the question of synthesis of closed circuit is well-researched of modern theory's automatic control, must pay attention to the synthesis of open circuit and solving insufficiently known its main tasks for formation of multi-frequency (multidimensional) information signal and for to control POS and identification of destabilizing impact factors (DIF). In the methodical plan is also important that the system is controlled with a combined basis for synthesis adaptive of systems without search, so that is the proposed approach has the possibility for further development [6].

The principal difference between the proposed formal model (Fig. 1) and traditional method is to measure the vector DIF **X**. The sensor unit **S** is connected directly to the input of controlled perturbations MFT (multi-dimensional object to control) (point a) in the traditional system.

In the proposed system are measurements DIF of carried by identifier **I** for directly observed vector $\mathbf{Y}_{C0}$ and a priori known characteristics **A** of the converter CCP (converter controlled perturbations). Without considering the vector's uncontrolled effects Θ is actually observed vector $\Delta\mathbf{Y}_C = \Delta\mathbf{Y}_{C0} + \Delta\mathbf{Y}_{UNC}$, that is leading to identification errors DIF.

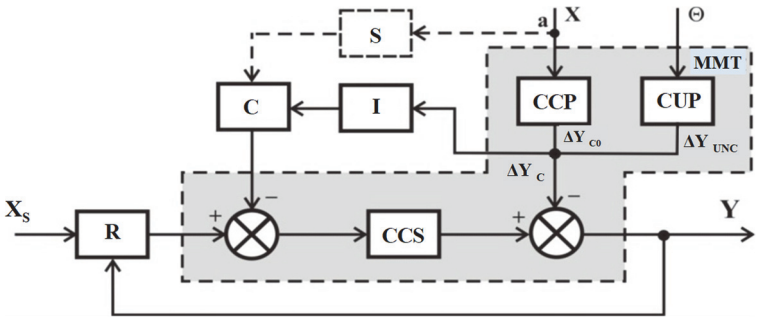

Fig. 1. The formalized model of invariant PRD: CCP – converter controlled perturbations, CCS – converter control signal, CUP – converter uncontrolled perturbation, I – identifier, C – compensator, R – regulator, S – sensor unit

We write the condition of invariance of the traditional system to:

$$\mathbf{K}_{C0} = \mathbf{W}^{-1}\mathbf{A}\mathbf{S}_0^{-1}, \tag{4}$$

where are $\mathbf{K}_{C0}$, $\mathbf{S}_0$ – the matrixes of the coefficient of transfer compensator (C) and the ideal sensor (S); $\mathbf{W}$ – the matrixes of the coefficient of signal for controlling.

In fact, there is always uncertainty $\mathbf{S} = \mathbf{S}_0 + \Delta\mathbf{S}$, which is equivalent to the uncertainty compensator $\Delta\mathbf{K}_S$. Then:

$$\mathbf{K}_{S0} + \Delta\mathbf{K}_S = \mathbf{W}^{-1}\mathbf{A}(\mathbf{S}_0 + \Delta\mathbf{S})^{-1}. \tag{5}$$

As $(\mathbf{S}_0 + \Delta\mathbf{S})^{-1} = [\mathbf{S}_0(\mathbf{E} + \mathbf{S}_0^{-1}\Delta\mathbf{S})]^{-1} = (\mathbf{E} + \mathbf{S}_0^{-1}\Delta\mathbf{S})^{-1}\mathbf{S}_0^{-1}$, where $\mathbf{E}$ – identity matrix, if $\|\mathbf{S}_0^{-1}\Delta\mathbf{S}\| \le \|\Delta\mathbf{S}\| \cdot \|\mathbf{S}_0^{-1}\| < 1$, than $(\mathbf{E} + \mathbf{S}_0^{-1}\Delta\mathbf{S})^{-1} = \mathbf{E} + \sum_{k=1}^{\infty}(-\mathbf{S}_0^{-1}\Delta\mathbf{S})^k$. Confining the first order of smallness in $\Delta\mathbf{S}$, we get:

$$\Delta\mathbf{K}_S = -\mathbf{W}\mathbf{A}\mathbf{S}_0^{-1}\Delta\mathbf{S}\mathbf{S}_0^{-1}. \tag{6}$$

The condition of invariance of the proposed system by $\mathbf{X}$ is written as:

$$\mathbf{K}_{I0} = \mathbf{W}^{-1}\mathbf{I}_0^{-1}. \tag{7}$$

Acting similarly, we get

$$\Delta\mathbf{K}_I = -\mathbf{W}^{-1}\mathbf{I}_0^{-1}\Delta\mathbf{I}\mathbf{I}_0^{-1}, \tag{8}$$

where $\Delta\mathbf{I}$ characterizes the uncertainty identification of impact factor.

Introducing the Euclidean norm and relative compensation uncertainty $\delta_{K_I} = \|\Delta\mathbf{K}_I\|/\|\mathbf{K}_{I0}\|$, $\delta_{K_S} = \|\Delta\mathbf{K}_S\|/\|\mathbf{K}_{S0}\|$, we get:

$$\delta_{K_S} = \|\mathbf{S}_0^{-1}\| \cdot \|\Delta\mathbf{S}\|, \quad \delta_{K_I} = \|\mathbf{I}_0^{-1}\| \cdot \|\Delta\mathbf{I}\|. \tag{9}$$

Given that fact, as $\mathbf{I}_0 = \mathbf{E}$ and $\mathbf{S}_0 = \mathbf{E}$, we get from Eqs. (6), (8) for the actual value of the system $\|\Delta\mathbf{S}\| \gg \|\Delta\mathbf{I}\|$, and therefore $\delta_{K_S} \gg \delta_{K_I}$ [6].

4. Developing invariant piezoresonance units with controlled dynamics

The architecture of invariant multi-frequency piezoresonance units (PRU) with controlled dynamics (IMPRU/CD) represented as adaptive controlling system with predictive reference model (Fig. 2) is considered. Its main component is the PRU core – multi-frequency

piezoresonance oscillatory system (MPOS) with supporting control circuits, interfacing, thermal and vibrational stabilization which is exposed to destabilizing disturbing factors. On the base of monitoring signals vector **Y** the system of optimal (suboptimal) assessment and identification accomplishes assessment of condition vector $\widehat{\mathbf{X}}_c$ and assessment of parameters' vector $\widehat{\mathbf{X}}_P$ of PRU mathematical model (parametric identification). The optimal control system, basing on reference model and current assessment of PRU condition vector, forms the vector of control signals **u**, thereby providing the system to move in accordance to specified optimization criteria and limits **L** related to distinguished physical implementation of MPOS. The control signal $\mathbf{u}'$ is also used by the optimal assessment and identification system (Fig. 2).

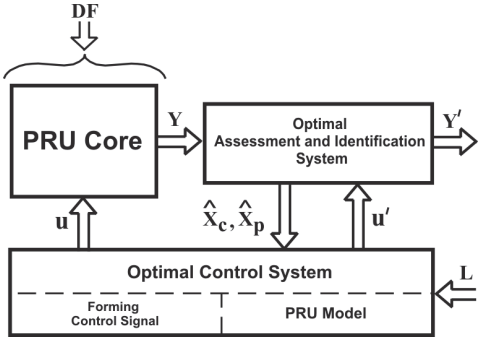

Fig. 2. The generalized architecture of IMPRU/CD

To identify optimal control criteria in accordance to the offered concept for creating IMPRU/CD the control process will be divided into two stages. At the first stage of the setting oscillation the control signal is formed in each excitation channel, which provides coming onto stationary mode for the shortest reachable time to set stable multi-frequency oscillation mode. At the second stage of the stabilizing oscillation the control signal is formed to support stability of generated oscillations in condition of destabilizing factors (providing technical invariance) [9-11].

The problem of control is defined as followed. The mathematical model of the system is specified as the differential equation system:

$$\dot{\mathbf{x}} = \Phi(\mathbf{x}, \mathbf{u}), \tag{10}$$

at initial condition:

$$\mathbf{x}(0) = \mathbf{x}_0, \tag{11}$$

where $\Phi = (\phi_1, \ldots, \phi_n)^T$ – vector function of the right part of the Eq. (10) of n dimension; $\mathbf{x} = (x_1, \ldots, x_n)$ – vector of phase coordinate of n dimension; $\mathbf{u} = (u_1, \ldots, u_k)$ – vector of control signals of k dimension.

The optimal control signal $\mathbf{u}(t)$ is to be found within $t \in [0, T]$ time period for system Eq. (10) at initial condition Eq. (11), providing for each excited oscillation mode the movement $x_i(t)$ at needed accuracy on the pass $x_i^*(t)$:

$$|x_i^*(t) - x_i(t)| \leq \varepsilon_i, \;\; i = \overline{1, n}, \tag{12}$$

where ε_i – specified tracking accuracy.

The movement pass $x_i^*(t)$ is defined by PRU reference model of the optimal control system (Fig. 2), which allows, on the basis of priori and current information of IMPRU/CD condition, defining the final time T^* and optimal pass for coming onto stationary mode of multi-frequency oscillations in accordance to criteria of time setting minimum [10, 11]:

$$\tau_{stat}^{opt} = \min_{\mathbf{P}\in\mathbf{D}} \max_{1\le i\le n} \tau_{stat_i}, \quad (13)$$
$$\mathbf{D} = \left\{\mathbf{P} \in \Re^N : p_{jmin} \le p_j \le p_{jmax},\ 1 \le j \le N\right\},$$

where τ_{stat_i} – time for setting stationary oscillation of mode i, defined by the specified longtime stability of oscillations δ_i, assuming structural specificity of PRU and its functionality; $\mathbf{P}_{min} = \{p_{1min}, \ldots, p_{Nmin}\}$, $\mathbf{P}_{max} = \{p_{1max}, \ldots, p_{Nmax}\}$ – specified vectors of minimal and maximal acceptable values of IMPRU/CD core parameters.

The problem Eqs. (10)-(13) may be considered as a problem of the terminal control according to which within the time T^* the system is to transit from initial condition $\mathbf{x}_0$ to terminal one:

$$\mathbf{x}(T^*) = \mathbf{x}_{T^*} : \mathbf{x}_0 \to \mathbf{x}_{T^*}. \quad (14)$$

In this case the optimal control algorithm is defined on the basis of minimizing the functional, which represents energy consumption of acceleration:

$$G(\mathbf{u}) = \frac{1}{2}\sum_{i,j}^{n} \left(\ddot{x}_i^*(t) - \ddot{x}_i(t,\mathbf{u})\right)\left(\ddot{x}_j^*(t) - \ddot{x}_j(t,\mathbf{u})\right). \quad (15)$$

From condition of reaching proximity to absolute minimum:

$$\min_G G(\mathbf{u}) = G(\mathbf{u}^*) = 0. \quad (16)$$

On control signals $\mathbf{u}$ [6].

Solving problems Eq. (13)-(16) in accordance to characteristics (physical properties) of PRU and its functionality is followed by limitations to oscillation amplitude U_i, initial frequency run-out $\Delta\omega_i$, maximal power of quartz resonator excitation P_{excit_Σ} and its increasing rate on the stage of setting multi-frequency mode for reducing thermal and dynamical instability of oscillation frequency:

$$\begin{aligned} &U_{min} \le U_i \le U_{max}, \\ &\Delta\omega_i \le \Delta\omega_{ultim},\ i = \overline{1,n}, \\ &P_{excit_\Sigma} \le P_{ultim},\ \frac{dP_{excit_\Sigma}}{dt} \le K_d^{(P)}. \end{aligned} \quad (17)$$

Upon reaching terminal condition Eq. (14) the system location relative to set condition $\mathbf{x}_{T^*}$ is stabilized. At this stage the minimizing functional Eq. (15) becomes:

$$G(\mathbf{u}) = \frac{1}{2}\sum_{i,j}^{n} \left(x_{T_i^*} - x_i(t,\mathbf{u})\right)\left(x_{T_j^*} - x_j(t,\mathbf{u})\right). \quad (18)$$

Providing minimizing deviation of the system $\Delta x_i = \left|x_{T_i^*} - x_i(t,\mathbf{u})\right|$, $i = \overline{1,n}$.

5. Strategy of optimal control for software trajectory motion of PRD with predictive model

The designed concept for invariant PRD like adaptive system with predictive standard requires solving inverse dynamics problem. It requires determination of the dynamic system motion and its parameters under a condition of performing of the motion corresponding to given trajectory. In accordance to specificity of development and exploiting IMPRU/CD control process is performed by two stages.

The first stage is the oscillation forming. Control impacts are formed in each exciting channels. The impacts provide the output to the stationary mode under a minimum time of set of stable multi-frequency oscillatory mode.

Second stage is the oscillation stabilization. Control of IMPRU/CD is directed to support of generated oscillations stability under influence of destabilizing factors, i.e. providing technical invariance [6].

We will carry out the construction of optimal or sub-optimal control law according to generalized work criterion that has good results at the stage of analytical construction during a designing period. Using this approach allows not only simplifier the procedure of obtaining the optimal control laws, but often do not obtain the functional dependences due to the cumbersomeness and complexity related to control laws. In such case, solving a problem comes to an end with an algorithm which performs optimization during system functioning and it is convenient from the point of view of a realization of microprocessor control.

Let us consider controlled process in the form of:

$$\dot{y}_i + f_i(x_1, \ldots, x_n, y_1, \ldots, y_m, t) = 0, \;\; \dot{x}_j = u_j, \tag{19}$$

where f_i is differentiable or piecewise differentiable functions; $\mathbf{x} = (x_1, \ldots, x_n)$ is the state vector of the control elements; $\mathbf{y} = (y_1, \ldots, y_m)$ is the state vector of the control object; $\mathbf{u} = (u_1, \ldots, u_m)$ is the control vector, $i = \overline{1,n}$, $j = \overline{1,m}$.

In considered case, the control of the rates related to the variations of controlled elements is performed. Object non-stationarity can be taken into account by extension its state vector.

Equation of system free movement Eq. (16) can be written as:

$$\dot{\mathbf{y}} + f(\mathbf{x}, \mathbf{y}, t) = 0, \;\; \dot{\mathbf{x}} = 0. \tag{20}$$

E.g. free system movement is the movement under fixed locations of the control elements.

For the task formulated by using an Eq. (19), we have expanded state vector $(\mathbf{x}, \mathbf{y})$. According to optimal controlling the minimum of the functional [11]:

$$I = V_{set}\big(\mathbf{x}(t_2), \mathbf{y}(t_2)\big) + \int_t^{t_2} Q(\mathbf{x}, \mathbf{y}, t)dt + \frac{1}{2}\int_t^{t_2} \sum_{j=1}^{m} \frac{u_j^2 + u_{jopt}^2}{k_j^2} dt. \tag{21}$$

Provides the control of the form of:

$$u_j = u_{j_{opt}} = -k_j^2 \frac{\partial V}{\partial x_j}, \tag{22}$$

where $V = V(y, t)$, is the solving the following equation:

$$\frac{dV}{dt} - \sum_{i=1}^{n} f_i \frac{dV}{dy_i} = -Q. \tag{23}$$

Under boundary condition of $V_{t=t_2} = V_{set}$; f_i, Q, where V_{set} are given uninterrupted functions; $k_j^2 > 0$ are given coefficients.

In order to provide prediction of object behavior, model of free movement must operate in faster mode as $t' = t/\chi$, where $\chi = const \gg 1$. Then, the equation of prediction model can be written as:

$$\frac{d\mathbf{y}_M}{dt'} + \chi \cdot f(\mathbf{x}_M, \mathbf{y}_M, \chi t') = 0, \quad \frac{d\mathbf{x}_M}{dt'} = 0. \tag{24}$$

A prediction model has to provide the integration of free movement during total optimization interval from $t = t_1$ till to t_2 by using faster rate under initial conditions given by control (estimation) system. Integration rate that defined by χ value is selected in such a manner that for each cycle of Δt_c (in many times less than $t_2 - t$) several runs of a free movement were performed during the interval of $t_2 - t$. The latter procedures are necessary for numerical evaluation the partial derivations $\partial V / \partial y_i$. Because of this, the values χ in real-life control of a process must be of the value equal to dozens, hundreds and even thousands units.

The beginning of each cycle coincides with current time moment t with accuracy equal to Δt_c. At the beginning of each cycle, control and estimation system operating with real-life controlled process defines the state vector $\mathbf{x}(t)$ and gives initial conditions for free movement model Eq. (22). As a result, the following equality is provided for beginning of each cycle:

$$\mathbf{y}_M(t) = \mathbf{y}(t). \tag{25}$$

Under free movement of the system, the left part of Eq. (23) transforms to the total derivative under time as:

$$\dot{V} = -Q. \tag{26}$$

Therefore, we obtain:

$$V\big(\mathbf{y}_M(t_2)\big) - V\big(\mathbf{y}_M(t_1)\big) = -\int_{t_1}^{t_2} Q(\mathbf{y}_M, t)dt, \tag{27}$$

and for a terminal task:

$$V\big(\mathbf{y}_M(t_2)\big) = V_{set}\big(\mathbf{y}_M(t_2)\big). \tag{28}$$

Thus, for free movement system mode under predictive model, the following computations must be performed:

$$V = V_{set}\big(\mathbf{x}_M(t'_2), \mathbf{y}_M(t'_2)\big) + \chi \int_{t'=t/\chi}^{t'_2=t_2/\chi} Q(\mathbf{x}_M, \mathbf{y}_M, \chi t')dt'. \tag{29}$$

In order to evaluate by using numerical technique the partial derivations $\partial V / \partial x_j$, the variability of initial requirement related to $\mathbf{x}_M$ is performed for each run of the model Eq. (24).

Let us consider the features necessary for selection of integrand for minimizing functional $Q(\bullet)$ given in the form Eq. (21). The features depend on the difference between output vector $\mathbf{y}_M$ contained in the model Eq. (24) and the estimate of the control process state $\hat{\mathbf{y}}$:

$$Q = Q(\mathbf{y}_M - \hat{\mathbf{y}}). \tag{30}$$

Let us introduce the square functional as:

$$Q = (\mathbf{y}_M - \hat{\mathbf{y}})^T \beta (\mathbf{y}_M - \hat{\mathbf{y}}), \tag{31}$$

where β is the diagonal matrix contained the elements that are proportional to the maximum errors

related to the corresponding coordinates (principle of the contribution of the errors).

By exploiting the optimal Kalman filter or suboptimal estimation procedure, it is necessary to define the following:

$$\beta = \widehat{\mathbf{R}}^{-1}, \tag{32}$$

where $\mathbf{R}$ is the error covariance matrix or their estimates $\widehat{\mathbf{R}}$.

It is also interesting an approach to forming the sequence of quality functional which describes the energy of system movement, for example, the minimum of acceleration energy as:

$$Q = \left(\mathbf{y}_M - \hat{\mathbf{y}}\right)^T \beta \left(\mathbf{y}_M - \hat{\mathbf{y}}\right). \tag{33}$$

This approach allows improving the dynamic accuracy for control of transmission processes in IMPRU/CD on the stage of oscillation reconstruction [6].

Several limitations exist for solving the task Eqs. (19)-(24) according to physical peculiarities and functional assignment of PRD (Eq. (17)).

In order to give limitations, expanded state vector $(\mathbf{x}, \mathbf{y})$ can be represented in the form of some space state domain G, which we will consider as enclosed and simply-connected. Let us give the penalty function $Q_f(\mathbf{x}, \mathbf{y})$, which is equal to zero inside and on the borders of the domain G and rather fast accrue in given domain. Assuming that the domain G is described by the equation $Q_f(\mathbf{x}, \mathbf{y}) = 0$, we represent the integrand function of the functional of quality related to generalized work Eq. (21) as:

$$Q = Q_{opt} + Q_f. \tag{34}$$

For what inside the domain of limitations $Q = Q_{opt}$. The function Q_{opt} is determined by the limitations of Eqs. (31)-(33) given inside the domain G, and the limitations of Eq. (34) are given for the minimized functional (21) with help of the penalty function Q_f Eq. (34).

It should be noted that described above algorithm corresponds to the terminal (quasi-terminal) control state $V_{t=t_{set}} = V_{set}$ which is related to the first control stage, e.g. forming stable and multi-frequency oscillating mode in IMPRU/CD. However, it can be simply transformed to the non-terminal algorithm of control by using transition to "sliding" optimization interval for which optimization interval is given as $t_2 = t + T_{\text{set}}$, where T_{set} is the given optimization interval. According to that, predictive model performs integration of the Eq. (24) within the interval from t/χ till to $(t + T_{set})/\chi$. As the function of V_{set} can be selected, an arbitrary function, including $V_{set} \equiv 0$.

After achievement the terminal state Eq. (28), stabilization of location of the system relatively given state is performed $V_0 \equiv V_{ST}$. For this reason, transition to the "sliding" optimization interval T_{ST} is executed.

Let us define productivity of control microprocessor system necessary for realization of technical invariance principle in PRD using adaptive system with predictive standard. If under condition of single-entry numerical integration for optimization interval equal to T_{ST} necessary N operations, then performance of microprocessor device can be approximately estimated as follows:

$$n_M = \frac{m+1}{2\Delta t_c} N. \tag{35}$$

It was assumed here that number of components of influence vector which give control process is equal to m and binary system of numerical differentiation is exploited. Value of Δt_c is defined by a necessary velocity of the update for given influences. For example, for $m = 3$, $\Delta t_c = 0.5$ s, $N = 2 \cdot 10^5$ microprocessor device must provide productivity in the level of $n_M = 8 \cdot 10^5$ operations

per one second [6, 11].

6. Mathematical model of multi-frequency piezoresonance oscillation system

High effectiveness of multi-frequency oscillating mode is provided by condition of high stability in generated oscillations. This is possible only with using filtering schemes in which QR is embedded in feedback circuit (FC) and is excited in the frequencies close to those of its own consequent resonances. At limited quantity of generated oscillations the other oscillator schemes can be used, for example those of oscillating type [12, 13].

The basic IMPRU/CD core architecture represents MPOS to have principles of creating filtering schemes implemented (Fig. 3). It incorporates passive multi-frequency quartz quadripole unit (MQU) on the base of quartz resonator with m-frequencies generating z_{q_j} and n excitation channels embedding the generalized non-linear component (NLC) and phasing selective feedback circuit (FBC). The automatic bias circuits with complex equivalent resistance z_{b_i} are used for stabilizing NLCi operational mode. The selective non-linear circuits FBC with gain $K_{ji}(jw, u_\Sigma, \tau)$, $j = \overline{1,m}$, $i = \overline{1,n}$, except for their function to set required amplitude-phase ratio in excitation channels, provide significant reducing competition in oscillations due to their own selective properties $K_{ji}(jw)$ and also automatic adjustment $K_{ji}(u_\Sigma)$ of oscillation amplitudes for fixing the specified (ultimately acceptable) power dissipation on QR.

Fig. 3 has the following symbols' identifications:

• $z_{in_\Sigma} = R_{in_\Sigma}/(1 + jw\tau_{in_\Sigma})$, $R_{in_\Sigma}^{-1} = \sum_i R_{in_i}^{-1}$, $C_{in_\Sigma} = \sum_i C_{in_i}$ – the complex equivalent total resistance of partial FC input circuits;

• $z_{out_\Sigma} = R_{out_\Sigma}/(1 + jw\tau_{out_\Sigma})$, $R_{out_\Sigma}^{-1} = \sum_i R_{out_i}^{-1}$, $C_{out_\Sigma} = \sum_i C_{out_i}$ – the complex equivalent total resistance of output NLC$_i$ circuits;

• $z_{ab_i} = R_{ab_i}/(1 + jw\tau_{ab_i})$ – complex resistance of auto-bias circuit i;

• $\tau_{ab_i} = R_{ab_i}C_{ab_i}$, $\tau_{in_\Sigma} = R_{in_\Sigma}C_{in_\Sigma}$, $\tau_{out_\Sigma} = R_{out_\Sigma}C_{out_\Sigma}$ – time constants;

• $i_\Sigma = \sum_i i_{out_i}(e_i)$ – total current of NLC$_i$; $e_i(\tau) = \sum_j v_i(\tau) + E_i + \tilde{E}_i(\tau)$ – control voltage in NLCi input, where E_i, $\tilde{E}_i(\tau)$– constant and variable components of auto-bias voltage;

• $u_\Sigma(\tau) = U_0(\tau) + \sum_j U_j(\tau) \cdot cos[w_j t + \varphi_j(\tau)]$– the total voltage in FC circuit input, where $U_j(\tau)$, w_j and $\varphi_j(\tau)$ – envelope, frequency and phase of oscillation j correspondently, $\tau = t - t_0$ – time interval from initial moment t_0 (MPOS startup moment) [6].

MPOS operation (Fig. 3) is described by the system of differential equations:

$$u_\Sigma = Z(p) \cdot \sum_i i_{out_i}\left(\sum_j K_{ji} \cdot u_\Sigma, \tilde{E}_i, E_i\right), \tag{36}$$

$$E_i = -z_{ab_i}(p) \cdot i_{out_i}\left(\sum_j K_{ji} \cdot u_\Sigma, \tilde{E}_i, E_i\right), \tag{37}$$

where:

$$Z(p) = \frac{z_{in_\Sigma}(p) z_{out_\Sigma}(p)}{z_{in_\Sigma}(p) + z_{out_\Sigma}(p) + z_q(p)}, \tag{38}$$

Is symbolic gain of MQU, representing control resistance of MPOS; $p \equiv d/dt$.

Representing control resistance $Z(p)$ Eq. (12) as the ratio:

$$Z(p) = \frac{\delta \cdot P(p,\delta)}{Q(p,\delta)}, \tag{39}$$

where $P(p,\delta)$, $Q(p,\delta)$ – polynomials of p; δ – low parameter, physically determined for resonance systems as damping ratio, and taking into account that in the general case solving system Eq. (36) is as sum of oscillations with frequencies close to resonance ones of QR ω_{q_j}:

$$u_\Sigma = \sum_{j=1}^{m} U_j(\tau)\cos(\omega_{q_j} t + \varphi_j(\tau)), \tag{40}$$

where $U_j(\tau)$ and $\varphi_j(\tau)$ – slowly changing parameters, the output current of NLCi with low parameter δ accuracy can be written as:

$$i_{out_i}(e_i) = I_{o\,i}(V_{ji}, E_i, \tilde{E}_i) + \sum_{j=1}^{m} I_{ji}(V_{ji}, E_i, \tilde{E}_i)\cos[\omega_{q_j} t + \psi_{ji}(t)], \tag{41}$$

where $I_{o\,i}$ – constant component; $I_{ji} = \bar{S}_{ji}(V_{ji}, E_i, \tilde{E}_i)V_{ji} = \bar{S}_{ji}(V_{ji}, E_i, \tilde{E}_i)U_j K_{ji}$; $\psi_{ji} = \varphi_j + \Delta\varphi_{ji}$; K_{ji}, $\Delta\varphi_{ji}$ – gain and phase shift of circuit i of FC for resonance frequency j of QR; $\bar{S}_{ji}(V_{ji}, E_i, \tilde{E}_i) = \frac{1}{V_{ji}} \underset{j}{L}\left[i_{out_i}(V_{ji}, E_i, \tilde{E}_i)\right]$ – mean slope for oscillation j; $\underset{j}{L}[\bullet]$ – mean operator.

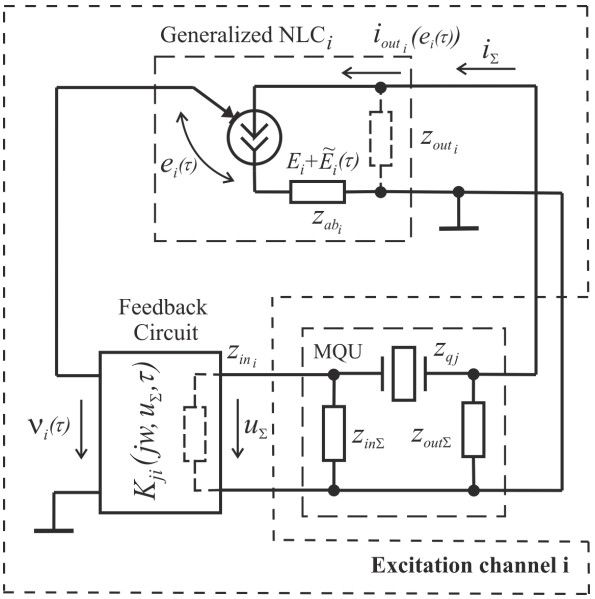

Fig. 3. The basic IMPRU/CD core architecture

Having entered complex amplitudes $\dot{U}_j = U_j \exp(j\varphi_j)$, $\dot{I}_{ji} = I_{ji}\exp(j\psi_{ji})$ and complex FC gain $\dot{K}_{ji} = K_{ji}\exp(j\Delta\varphi_{ji})$, and split real and imaginary units the reduced equations for amplitudes, MPOS oscillation phases and auto-bias voltages become [6, 12, 13]:

$$T_j \frac{dU_j}{dt} = \left[R_{e_j} K_{\phi_j} \sum_{i=1}^{n} \bar{S}_{ji}(V_{ji}, \tilde{E}_i, E_i) \cdot K_{ji}\cos(\Delta\varphi_{ji} + \Delta_{\phi_j}) - 1\right] \cdot U_j, \tag{42}$$

$$T_j \frac{d\varphi_j}{dt} = R_{e_j} K_{\phi_j} \sum_{i=1}^{n} \bar{S}_{ji}(V_{ji}, \tilde{E}_i, E_i) \cdot K_{ji} \sin(\Delta\varphi_{ji} + \Delta_{\phi_j}) - \Delta\omega_j T_j, \quad (43)$$

$$T_{ab_i} \frac{d\tilde{E}}{dt} = -\left[R_{ab_i} I_{0i}\left(V_{ji}, \tilde{E}_i, E_i\right) + \tilde{E}_i\right], \quad (44)$$

or as generalized matrix:

$$\mathbf{T} \frac{d\mathbf{U}}{dt} = \left[\mathbf{G}_R \cdot \mathbf{R} - \mathbf{E}_{(mm)}\right] \cdot \mathbf{U}, \quad (45)$$

$$\mathbf{T} \frac{d\Phi}{dt} = [\mathbf{G}_I \cdot \mathbf{R} - \Delta] \cdot \mathbf{E}_{(m1)}, \quad (46)$$

$$\mathbf{T}_{ab} \frac{d\tilde{\mathbf{E}}}{dt} = -\left(\mathbf{R}_{ab} \cdot \mathbf{I}_0 + \tilde{\mathbf{E}}\right), \quad (47)$$

where $\mathbf{T} = diag(T_1, \ldots, T_m)$, $\mathbf{T}_{ab} = diag(\tau_{ab_1}, \ldots, \tau_{ab_n})$ – time constant matrixes of partial oscillation system $T_j = 2/\omega_{q_j}\delta_j$ of $m \times m$ dimensions and auto-bias circuits NLCi of $n \times n$ dimensions; $\mathbf{U} = (U_1, \ldots, U_m)^T$, $\Phi = (\varphi_1, \ldots, \varphi_m)^T$ and $\tilde{\mathbf{E}} = (\tilde{E}_1, \ldots, \tilde{E}_n)^T$ – vectors of oscillation amplitudes and phases of m dimension and vector of auto-bias voltage of n dimension; $\mathbf{G}_R = \mathrm{Re}\dot{\mathbf{G}} = \left|\dot{\mathbf{G}}\right|\cos\Delta\varphi^T$, $\mathbf{G}_I = \mathrm{Im}\dot{\mathbf{G}} = \left|\dot{\mathbf{G}}\right|\sin\Delta\varphi^T$ – matrixes of real and imaginary units of equivalent complex conductance of active part of MPOS $\left|\dot{\mathbf{G}}\right| = \left(\bar{S}_{ji}K_{ji}\right)_{j=1,i=1}^{m,n}$ of $m \times n$ dimensions; $\mathbf{R} = \mathbf{R}_e \cdot \mathbf{K}_\phi$ – matrix of reduced resistances; $\mathbf{R}_e = diag\left(R_{e_1}, \ldots, R_{e_m}\right)$ – matrix of equivalent resistances $R_{e_j} = R_{in_\Sigma} \cdot R_{out_\Sigma}/(R_{in_\Sigma} + R_{out_\Sigma} + R_{q_j})$ of $m \times m$ dimensions, $\mathbf{K}_\phi = diag\left(K_{\phi_1}, \ldots, K_{\phi_m}\right)$ – matrix of equivalent phase link gains $K_{\phi_j} = 1/\sqrt{1 + (\omega_{q_j} \cdot T_{\phi_j})^2}$, $T_{\phi_j} \approx R_{in_\Sigma}(C_0 + C_{in_\Sigma}) + R_{out_\Sigma}(C_0 + C_{out_\Sigma})$ – time constant of equivalent phase link, providing phase shift $\Delta\varphi_{\phi_j} = -\mathrm{arctg}(\omega_{q_j} \cdot T_{\phi_j})$ between immediate values of voltage $u(t)$ and current $i(t)$; ω_{q_j}, C_0 – resonance frequency and parallel capacity of QR; $\Delta\varphi = \left(\Delta\varphi_{ji} + \Delta\varphi_{\phi_j}\right)_{j=1,i=1}^{m,n}$ – matrix of $m \times n$ dimensions, which provides phase relations in excitation channels of MPOS; $\Delta = diag(\Delta\omega_1 T_1, \ldots, \Delta\omega_m T_m)$ – matrix of generalized detuning, $\Delta\omega_j = \omega_{q_j}^2 \left(R_{in_\Sigma}\tau_{in_\Sigma} + R_{out_\Sigma}\tau_{out_\Sigma}\right)/2Q_{q_j}R_{q_j}$ – frequency adjustment to oscillation j explained by the fact that reduction was produced relative to natural frequencies of QR ω_{q_j} with no respect to phase-shift in FC circuits; Q_{q_j}, R_{q_j} – quality factor and dynamic resistance of QR for oscillation frequency j; $\mathbf{R}_{ab} = diag(R_{ab_1}, \ldots, R_{ab_n})$ – matrix of auto-bias resistance of $n \times n$ dimensions; $\mathbf{I}_0 = (I_{0_1}, \ldots, I_{0_n})^T$ – vector of constant components of output currents $i_{\mathrm{out}_i}(e_i)$; $\mathbf{E}_{(mm)}$, $\mathbf{E}_{(m1)}$ – unit matrix of $m \times m$ dimensions and unit column vector $m \times 1$; m – quantity of generating frequencies, n – quantity of excitation channels.

7. Dynamics of multi-frequency piezoresonance oscillation system

The case considers three-frequency excitation of the main mode of oscillations of multi-frequency QR and two additional ones – informative: temperature and vibration ($m = n = 3$) [6, 14]. At polynomial approximation the output current of NLCi (Fig. 2) can be represented as:

$$i_{out_i}(e_i) = I_s \left[\hat{a}_0 + \sum_{r=1}^{k} \hat{a}_r(\hat{v}_i + X_{b_i})^r\right], \quad i = \overline{1,n}, \quad k = 3{,}5, \quad (48)$$

where $\hat{v}_i = v_i \cdot S_0/I_s$ – normalized control voltage; $X_{b_i} = \bar{x}_{b_i} + \tilde{x}_{b_i}$, $\bar{x}_{b_i} = (E_i - E_s) \cdot S_0/I_s$, $\tilde{x}_{b_i} = \tilde{E}_i \cdot S_0/I_s$ – constant and variable components of normalized bias; $\hat{a}_0 = a_0/I_s$, $\hat{a}_r = a_r \cdot I_s^{(r-1)}/S_0^r$ – normalized coefficients of approximating polynomial; I_s, E_s – the coordinates of the point in the center of volt-amps diagram (VAD) with maximal gain slope S_0.

Having used trigonometry formulas of multiple argument and averaging accordantly to Eq. (41), the spectral components in NLCi input at approximation by polynomial of the third degree will be written as:

$$I_{ji} = V_{ji} \cdot \overline{S}_{ji} = V_{ji} \cdot S_0\left[A_{1_i} + 0{,}75 \cdot \hat{a}_3 B_{1_i}\right], \tag{49}$$

$$I_{0_i} = I_s\left[A_{2_i} + 0{,}5\left(\hat{a}_2 + 3\hat{a}_3 X_{b_i}\right)B_{2_i}\right]. \tag{50}$$

Having substituted the expressions (49), (50) into reduced Eqs. (42)-(44) and assuming $K_{\phi_j} \approx 1$ and $\Delta\varphi_{\phi_j} \approx 0$, the three-frequency MPOS ($m = 3$) motion equation with three non-linear components ($n = 3$) will be obtained:

$$\xi_j \frac{d\widehat{U}_j}{d\hat{t}} = S_0 R_{e_j} K_{jj} \cdot \widehat{U}_j \left(\sum_{i=1}^{3} \left(A_{1_i} + 0{,}75\hat{a}_3 B_{1_i}\right) \cdot \gamma_{ji}^2 \frac{K_{ii}}{K_{jj}} - \frac{1}{S_0 R_{e_j} K_{jj}} \right), \tag{51}$$

$$\xi_j \frac{d\varphi_j}{d\hat{t}} = S_0 R_{e_j} K_{jj} \cdot \sum_{i=1}^{3} \left(A_{1_i} + 0{,}75\hat{a}_3 B_{1_i}\right) \cdot \gamma_{ji} \sqrt{1 - \gamma_{ji}^2} \frac{K_{ii}}{K_{jj}} - \xi_j \Delta\omega_j, \tag{52}$$

$$\mu_i \frac{dX_{b_i}}{d\hat{t}} = -S_0 R_{ab_i} \cdot \left(A_{2_i} + \frac{X_{b_i}}{S_0 R_{ab_i}} + 0{,}5\left(\underline{a}_2 + 3\underline{a}_3 X_{b_i}\right)B_{2_i} \right) + \bar{x}_{b_i}. \tag{53}$$

The correspondent Eqs. (51)-(53) at approximating transfer characteristics by polynomial of the fifth degree (48) are given in [6].

The following symbols used in Eqs. (51)-(53) stand for:

$$A_{1_i} = \sum_{r=1}^{3} r\hat{a}_r \cdot X_{b_i}^{(r-1)}, \quad A_{2_i} = \hat{a}_0 + \sum_{r=1}^{3} \hat{a}_r \cdot X_{b_i}^r,$$

$$B_{1_i} = K_{ii}^2 \sum_{k=1}^{3} b_{kij} \cdot \widehat{U}_k^2, \quad B_{2_i} = K_{ii}^2 \sum_{j=1}^{3} \gamma_{ji}^2 \cdot \widehat{U}_j^2.$$

$b_{kij} = \gamma_{ki}^2$, for $k = j$ and $b_{kij} = 2\gamma_{ki}^2$, for $k \neq j$; $\gamma_{ji} = \frac{K_{ji}}{K_{ii}} = \cos\Delta\varphi_{ji}$ – coefficients of suppressing inter-channel interference (parasite) oscillations ($j \neq i$); $\widehat{U}_j = S_0 U_j/I_s$ – normalized voltage in MQU output; $\xi_j = \frac{T_j}{\max\limits_{1\leq j\leq 3} T_j}$, $\mu_i = \frac{T_{ab_i}}{\max\limits_{1\leq j\leq 3} T_j}$ – normalized time constants of partial oscillation system j and bias circuit i; $\hat{t} = \frac{t}{\max\limits_{1\leq j\leq 3} T_j}$ – normalized time; $j = \overline{1,3}$, $i = \overline{1,3}$.

Activity of excited oscillations is determined by regeneration parameter to be found from (51) when $\widehat{U}_j = 0$:

$$K_j^{reg} = R_{e_j} K_{jj} S_{s_j} = R_{e_j} K_{jj} S_0 \times \sum_{i=1}^{3} \left(\sum_{r=1}^{3,5} r\hat{a}_r X_{s_j}^{(r-1)} \right) \gamma_{ji} \frac{K_{ii}}{K_{jj}}, \tag{54}$$

where S_{s_j} – gain slope of volt-amps diagram in still point for oscillation j; X_{s_j} – bias in the still

point for NLCi, being the solution for non-linear equation:

$$S_0 \cdot R_{ab_i}\left(\hat{a}_0 + \frac{X_{b_i}}{S_0 \cdot R_{ab_i}} + \sum_{r=1}^{3} \hat{a}_r \cdot X_{b_i}^r\right) - \bar{x}_{b_i} = 0. \quad (55)$$

Figs. 4, 5 shows distinguished case of stabilizing oscillations in three-frequency MPOS, as result of numerical integrating Eqs. (51)-(53). The bipolar transistors KT368 (2SC9018) are used as active components (NLCi), which have average statistical values of VAD parameters: $S_0 = 0.1$ A/V; $\hat{a}_0 = 0.95$; $\hat{a}_1 = 0.55$; $\hat{a}_2 = 0.051$; $\hat{a}_3 = -0.054$, when approximation error $\varepsilon \leq 5$ %. Initial values of low-varying parameters made: $T_j = 0.1$ s; $T_{ab_i} = 1 \cdot 10^{-4}$ s; $R_{ab_i} = 1$ kΩ; $K_{jj} = -20$ dB; $\bar{x}_{b_i} = 30$.

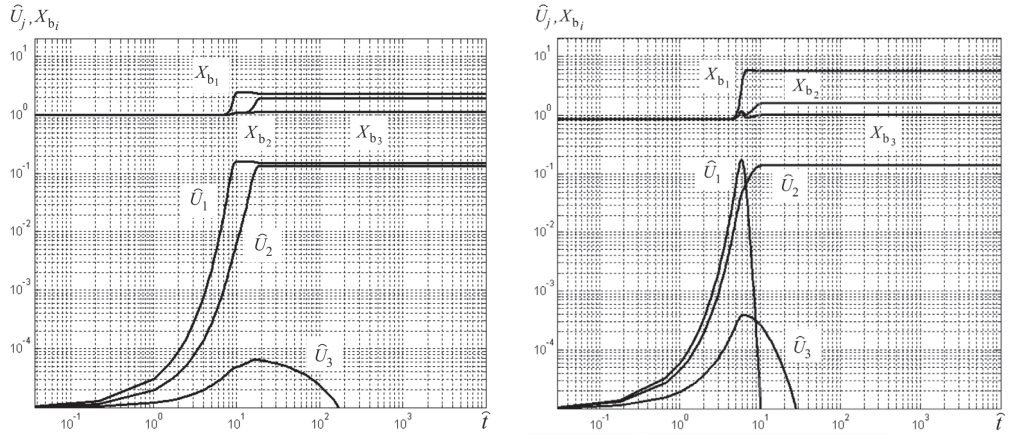

Fig. 4. Distinguished case of appearing competition of oscillations in excitation channels of MPOS: a) suppressing energetically less active oscillations, b) suppressing energetically more active oscillation by less active one

It's obvious that high competition in excitation channels ($\gamma_{ji} = -6$ dB) can bring to situations when oscillations with low energetic activity (oscillation $\hat{U}_3$, Fig. 4(a), (b)) can be suppressed by more active oscillations (with high regeneration coefficient K_j^{reg}). At the same time the overly high increasing regeneration parameter K_j^{reg} can cause a breakdown of more energetically active oscillations (oscillation $\hat{U}_1$, Fig. 4(b)) in excitation channels of MPOS. Reducing competition of oscillations due to increasing selective properties of FC circuits down to $\gamma_{ji} = -12$ dB provides stable three-frequency mode of oscillation (Fig. 5 (a)) even when regeneration coefficient values $K_1^{reg} = 1.25$, $K_2^{reg} = 1.5K_3^{reg}$ are growing significantly [6, 14, 15].

In this case it assumes using the term of low or high active oscillation (oscillations) in relation to the other oscillations of MPOS, which, being energetically all-sufficient in one-frequency mode, may fade on transiting to multi-frequency mode of oscillations in the certain conditions.

Fig. 6(a) represents approximated relationships of oscillation stabilizing time $\tau_{stat} = \max\limits_{1 \leq j \leq m} \tau_{stat_j}$ at various partial coefficients of FC. It also has bifurcation curve that determines a range of stable MOM. Evidently, at high values of variations $\chi = \max\limits_{1 \leq j \leq m} K_j^{reg} / \min\limits_{1 \leq j \leq m} K_j^{reg} = \max\limits_{1 \leq j \leq m} R_{e_j} / \min\limits_{1 \leq j \leq m} R_{e_j}$ of regeneration coefficients the oscillation stabilizing time τ_{stat} is significantly increasing (by an order and more!). Compensation of this events when having the great scatter of equivalent resistances R_{e_j} is possible by selecting appropriate coefficients K_{jj} of partial FC (increasing energy of oscillations), what it's not only

improving dynamic properties of MPOS, but also brings to extending range of stable MOM (Fig. 6(a)).

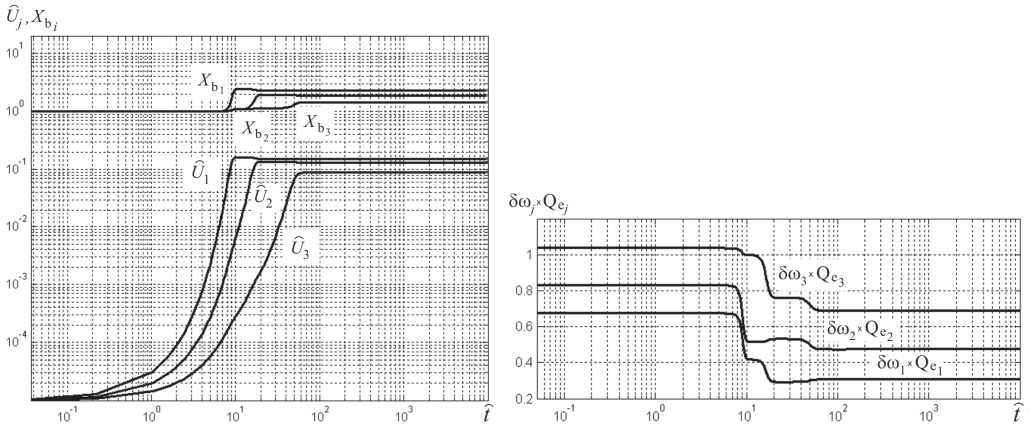

a) b)

Fig. 5. Stable three-frequency oscillation mode: a) setting oscillation amplitudes and auto-bias voltages, b) initial run-out of oscillation frequencies, caused by amplitude and phase conversion in excitation channels

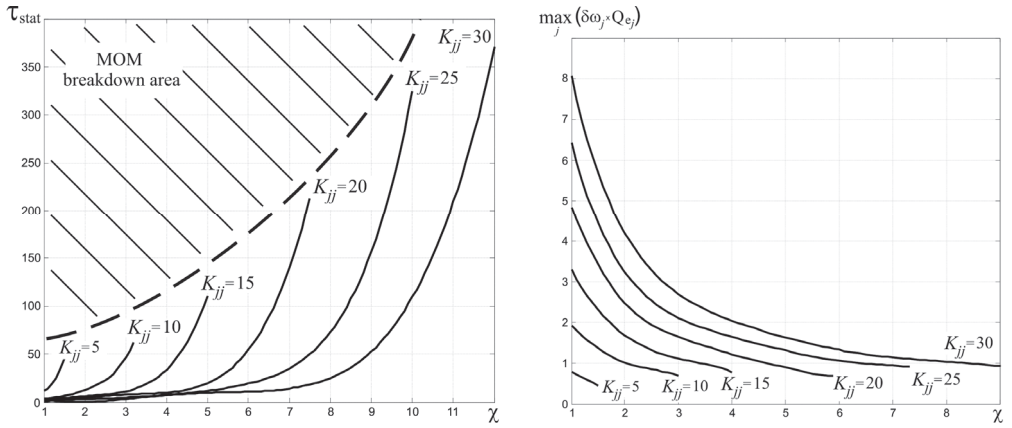

a) b)

Fig. 6. a) Dependences of normalized oscillation stabilizing time and b) initial frequency run-out on MPOS parameters

The quite important characteristic of MPOS dynamics is group run-out of oscillation frequencies $\delta\omega_j Q_{e_j}$, which is defined according to Eq. (52). The modeling results indicate that amplitude-phase conversion slightly exhibits for energetically "weak" oscillations (Fig. 5(b)). At joint control of oscillation amplitude and voltage of auto-bias the relative run-out of frequencies $\delta\omega_j = \left(\omega_{q_j}\right)^{-1} \cdot \Delta\omega_j(\hat{t}) = \left(\omega_{q_j}\right)^{-1} \cdot \frac{d\varphi_j}{d\hat{t}}$ may reach values from 10^{-8} to 10^{-6}, and significantly reduce on increasing coefficients K_{jj} of partial circuits of FC (Fig. 6(b)).

8. Strategy ground for optimal parameters search in MPOS

A. General statement of PRD parametric synthesis.

In the general statement of MPOS parametric synthesis the required solution will be found by criterion Eq. (13):

$$\tau_{set}^{opt} = \min_{\lambda \in D} \tau_{set}(\lambda), \quad D = \{\lambda \in R^N : \lambda_{i_{min}} \le \lambda_i \le \lambda_{i_{max}}, 1 \le i \le N\} \tag{56}$$

where duration of transient process τ_{set} is determined by solving Eqs. (51)-(53); $\lambda_{min} = \left(\lambda_{1_{min}}, \ldots, \lambda_{N_{min}}\right)$, $\lambda_{max} = \left(\lambda_{1_{max}}, \ldots, \lambda_{N_{max}}\right)$ – vectors set for minimally and maximally acceptable values of parameters of MPOS circuits.

Taking into account that the requirements to expanding stable oscillation range and shortening transient process duration become in contradiction with requirements to stability of generated oscillations poses additional limitations to values of oscillation amplitudes and initial frequency deflections $\widehat{U}_j$ and $\delta\omega_j$ Eq. (17):

$$\max_{1 \le j \le m} \widehat{U}_j \le \widehat{U}_{lim}, \quad \max_{1 \le j \le m} \widehat{U}_j / \min_{1 \le j \le m} \widehat{U}_j \le l, \quad \max_{1 \le j \le m} \delta\omega_j \le \delta\omega_{lim}, \tag{57}$$

where $\max_{1 \le j \le m} \widehat{U}_j$, $\min_{1 \le j \le m} \widehat{U}_j$ – maximal, minimal values of MPOS oscillation amplitudes; $\widehat{U}_{lim}$ – maximal limit of oscillation amplitudes, which is determined by maximally acceptable dissipation power in QR; l – coefficient that defines maximally acceptable amplitude difference $\widehat{U}_j$, normally $l = (1.5,\ldots,3)$ [13-15].

To solve synthesis problem (56), (57) the following circumstances are considered:

– high complexity of the optimization object, that often prevents analytical finding interconnection between oscillation setup time τ_{set} and MPOS parameters vector λ;

– complex, non-linear and possibly multi-extreme character of the objective function at the large number of limitations;

– large number of possible vector λ parameters, wide diapason of their vibration, therewith initial values of parameters can be outlying the optimal range;

– necessity of considering parameter scatter for real elements and calculation errors, and providing physical realization of MPOS.

B. Method for optimal parameter search in MPOS.

All existing methods for solving optimization problems can actually be divided into two groups: methods based on using as values of function to be minimized so its derivatives (gradient, first or second order methods); and algorithms, which use only values of function to be minimized (non-gradient or direct search methods).

Considering specificity of MPOS (51)-(53) dynamics equations for solving parametric optimization problem the most acceptable methods are direct search methods (non-gradient), which are based on calculation of only values of objective function. Ones of the most effective direct search methods are simplex methods, which can be easily modified for solution of conditional optimization problems (for example, S^2 – method or Hooke-Jeeves method) [16].

For parametric synthesis of PRD in the mode of quartz resonator multi-frequency excitation the modified method of S^2 or method of complexes is used. The basis of this method is building regular simplex, which is represented in N-dimensional space as polyhedron built by $N + 1$ points – vertexes equally distanced from one another. For example, in case of two variables the correct simplex is equilateral triangle, and in three-dimensional space – tetrahedron.

To build new simplex on the plane the vertex with highest value of the objective function is moved to the needed distance along the line, which is drawn through the gravity center of other vertexes of simplex. The point obtained in this way is the vertex of new simplex, and the vertex selected in initial simplex is excluded. Therewith only one additional value of objective function is to be calculated. The search is finalized when simplex dimensions or differences in function

values in vertexes become quite small values, which are determined by maximally acceptable error tolerance.

Realization of complex method requires the following operations. The rigid acceptable point λ_0, reflection parameter β (recommended value $\beta = 1.3$) and calculation errors ε and δ are set in advance.

C. Building initial complex.

1) Finding coordinate λ_i^N:

$$\lambda_i^N = \lambda_0^N + \Xi_i^N, \;\; i = \overline{1,S}, \tag{58}$$

where Ξ^N – vector-row of evenly distributed numbers of N dimension, for each the following is true $\|\Xi^s\| \ll R$; R – radius of gravity hyperbole of the objective function minimum; $S = N + 1$.

2) Finding center of gravity: if λ_i^N – unacceptable point, then center of gravity is found for previously found points:

$$\hat{\lambda} = \frac{1}{i}\sum_i \lambda_i^N, \tag{59}$$

and assumption is made that:

$$\lambda_{i_{new}}^N = \lambda_i^N + 0.5\left(\hat{\lambda} - \lambda_i^N\right). \tag{60}$$

Procedure is repeated until $\lambda_{i_{new}}^N$ becomes acceptable.

The operations (C1, C2) are repeated until sufficient number of points is obtained ($i = S$), then the setup time is defined as $\tau_{set_i}(\lambda_i^N)$.

D. Complex reflection.

1) Point selection λ_{max}^N:

$$\tau_{max} = \tau_{set}(\lambda_{max}^N) = \max_i \tau_{set_i}(\lambda_i^N). \tag{61}$$

2) Finding gravity center $\hat{\lambda}$ and next point:

$$\lambda_{repl}^N = \hat{\lambda} + \beta\left(\hat{\lambda} - \lambda_{max}^N\right). \tag{62}$$

3) Verification of the conditions: if λ_{repl}^N – acceptable point and $\tau_{set}(\lambda_{repl}^N) < \tau_{max}$, the verification of conditions (E) is proceeded;

4) Verification of the conditions: if λ_{repl}^N – unacceptable point or $\tau_{set}(\lambda_{repl}^N) \geq \tau_{max}$, the distance between λ_{repl}^N and gravity center $\hat{\lambda}$ is two times reduced, the search is continued until condition (D3) is fulfilled.

E. Verification of the conditions of finalizing calculations.

1) Definitions:

$$\langle \tau_{set} \rangle = \frac{1}{S}\sum\nolimits_{i=1}^{S} \tau_{set_i}, \;\; \langle \lambda^N \rangle = \frac{1}{S}\sum\nolimits_{i=1}^{S} \lambda_i^N. \tag{63}$$

2) Verification of the conditions; if:

$$\sum\nolimits_{i=1}^{S} \left(\tau_{set_i} - \langle \tau_{set} \rangle\right)^2 \leq \varepsilon, \;\; \|\lambda_i^N - \langle \lambda^N \rangle\| \leq \delta, \tag{64}$$

then calculation is completed; otherwise transition to (D1) is proceeded [6].

9. Finding optimal parameter vector of MPOS

The parametric optimization of MPOS will be performed, so that three-frequency quartz resonator is realized as AT-cut of resonator with basic resonance frequency $f_{q_1} = 10009987$ Hz, quality factor $Q_{q_1} = 103000$, dynamic resistance $R_{q_1} = 24$ Ω, frequencies of two anharmonics $f_{q_2} = 10197018$ Hz and $f_{q_3} = 10268125$ Hz, quality factors $Q_{q_2} = 84000$, $Q_{q_3} = 61000$ and dynamic resistances $R_{q_2} = 60$ Ω and $R_{q_3} = 120$ Ω correspondently.

The optimization parameter vector $\lambda = (X_{s_i}, K_{jj})$ will be embedded by values, which determine direct current operation mode for non-linear elements and amplifying partial circuits of the feedback (FB). The selected features of FB circuits are fixed at level $\gamma_{ji} = -10$ dB, what provides acceptable stability for multi-frequency generation mode. The variation diapason for value $X_{S_i} \in [-0.6; -1.5]$ is selected by design considerations, what is equivalent to changes of R_{ab_i} in diapason (650, …, 2500) Ω.

The initial approach point (Fig. 7) is selected to the point which corresponds to generator nominal parameters: $\lambda_0 = (-1; 20)$; $\tau_{set_0}(\lambda_0) = 34.31$. According to optimization algorithm the problem of dimension $N = 2$ requires building three points of initial simplex, each of which $\lambda_i = (\lambda_1^{(i)}, \lambda_2^{(i)})$ can be obtained from the following relations:

$$\lambda_1^{(i)} = -1.5 + 0.9 \cdot \xi_1^{(i)}, \ \ \lambda_2^{(i)} = 5 + 25 \cdot \xi_2^{(i)}, \tag{65}$$

where $\xi_1^{(i)}$ and $\xi_2^{(i)}$ – random numbers, which are evenly distributed in the interval [0; 1].

The assumption is made that random numbers generator generates $\xi_1^{(1)} = 0.9$ and $\xi_2^{(1)} = 0.5$. Then $\lambda_1 = (-0.69; 17.5)$. This point is acceptable and memorized as the first point.

The next assumption is made that sensor generates $\xi_1^{(2)} = 0.27$ and $\xi_2^{(2)} = 0.2$. Then $\lambda_2 = (-1.26; 10)$. This point is unacceptable, so moving towards to gravity center of already found vertexes gives:

$$\hat{\lambda}_0 = 0.5(\lambda_0 + \lambda_1) = (-0.845; 18.75). \tag{66}$$

New point $\lambda_{2_{new}}$ is acceptable and memorized.

Final assumption is made that $\xi_1^{(3)} = 0.33$, $\xi_2^{(3)} = 0.7$. Then $\lambda_3 = (-1.2; 22.5)$. Next point is found by reflection:

$$\lambda_4 = \hat{\lambda}_1 + 1.3\left(\hat{\lambda}_1 - \lambda_{2_{new}}\right) = (-0.843; 27.31). \tag{67}$$

This point is unacceptable. Therefore, consequently moving towards to gravity center $\hat{\lambda}_1$ new point is found as $\lambda_{4_{new}} = (-0.93; 21.82)$, which is acceptable and memorized (Fig. 7).

Next operations return optimal parameter vector of generator λ^*. Continuing iteration processes does not result in changes of gravity center location (Fig. 7). Stopping calculations for the value $\varepsilon = 0.01$ results in vector of optimal values for MPOS $\lambda^* = \left(X_{S_i}^*, K_{jj}^*\right) = (-1.157; 26.61)$ and values $\tau_{set}^*(\lambda^*) = 11.27$.

Thus, as result of two-directional optimization of MPOS parameters the multi-frequency oscillations mode setup process duration reduced from 0.082 s to 0.0225 s (more than by three times in comparison with input value). At the same time changing only one parameter (increasing K_{jj} to value 23.7 or X_{S_i} to –0.6) the gain is obtained only by two times or at 95 % correspondently.

The gravity center movement trajectory and also rapid convergence of the iterative process to the point of MPOS parameter optimal values approves high efficiency of applied optimization

method. Noteworthy is that efficiency of parametric optimization significantly increases if the preliminary study of objective function is performed, for example, by brute-force search method [6, 12-15].

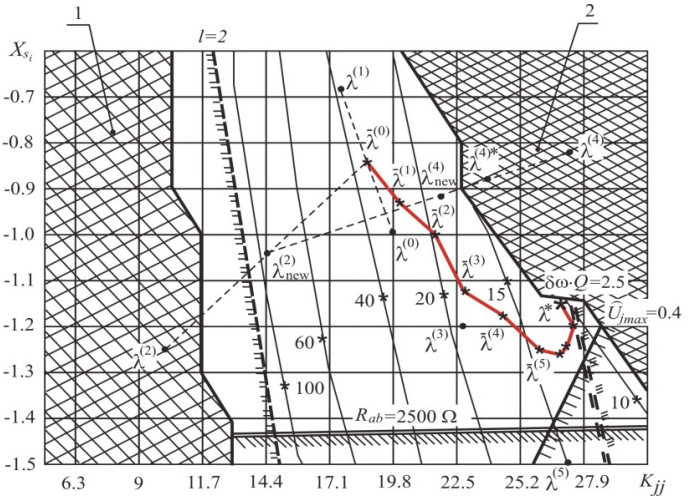

Fig. 7. Finding optimal parameter vector of MPOS: 1, 2 – break areas of multi-frequency oscillation mode

10. Conclusions

The offered approach to developing piezoresonance units with controlled dynamics, which are represented as the adaptive control system with predictive reference model, allows creating the new class of PRU to be invariant to disturbing destabilizing factors. This approach grounds on the principle of using natural redundancy in multi-frequency basis of PRU core – multi-frequency piezoresonance oscillation system what allows on the base of invariance theory not only synthesizing system with current identification of disturbing factors, but also adapting PRU relative to their effect.

The presented model invariant formalized PRD involves review in linear approximation. Accounting anisochronism and parametric phenomena POS calls for the use of non-linear approach, which is in the part of invariance has a number of significant features.

In particular, the terms of compensation for nonlinear combined system must perform more complex functions than linear. You need to take into account not only the influence of perturbing factors, and some coordinate system. This requirement cannot be nominated if in the invariant device the linear object only in relation to perturbation. In this case compensator must contain the same nonlinearity, as direct circle of influence disturbance, that circle of the direct influence of perturbation. Conditions invariance is to provide symmetry impact perturbation X on vector output Y, and it is determined almost the same as in linear systems.

Using of suggested conceptual states related to design invariant multi-frequency piezo-resonance devices with controlled dynamics in the form of adaptive-self-tuning systems with the fast operating predictive standard provided creation of novel class invariant PRD which accuracy performance is of maximum close to potentially possible level. Control the trajectory operating in a real-time environment is performed on the basis of predictive numerical analysis of the core dynamics in IMPRU. Model parameters are given corresponding to the results of identification of current state QR under multi-mode excitation and taking into account the constructive peculiarities of PRD concrete type.

In order to provide given system operation mode under its incomplete parametrical distinctness (robustness), two-stage interval-approximation control law has been developed. The law provides dividing the process into the sequence interval-local approximation tasks within the limits of two

stages for restoration and stabilization of multi-mode oscillation mode. During the first stage, adaptive control task is solved for each separate mode of IMPRU in order to provide operating the system under stationary oscillation mode in minimum time. During the second stage, control influences are formed. The latter ones are directed to the system stabilization under influence of destabilizing factors, i.e. providing technical invariance. Criteria for an optimal control in IMPRU/CD are analytically designed. That provides for each stage the minimization of energy expenses for optimal system operating trajectory. Local and global stability of interval-approximation control technique IMPRU/CD is demonstrated. Estimate of productivity of digital control system in IMPRU/CD confirms opportunity of physical realization of given conception by using wide spread ARM processes.

Using the developed mathematical model MPOS having in its base reduced differential equations for amplitudes, phases and voltages of auto-bias as predictive reference model of PRU core allows accomplishing effective controlling IMPRU/CD in accordance to the criteria of minimum of energy consumption as at the stage of setting multi-frequency oscillation mode so at the stage of stabilizing multi-frequency oscillations.

Method of complexes, which is related to direct search methods can be effectively used for parametric optimization of MPOS as in the project stage so in the stage of system functioning with purpose of its adaptation to external destabilizing factors. This method has certain advantages:

– logical structure of the method and necessary calculations are distinguished by simplicity and therefore its software realization is not complicated;

– low level of requirements to memory size of microcomputer and minor quantity of preliminary parameters to be installed;

– efficiency of the method is provided even when objective function calculation error is high, because while reflecting of the complex the highest value of objective function and gravity center $\hat{\lambda}$, which is obtained by averaging, are used.

Nevertheless, application of method of complexes is to consider some of its features:

– because all coordinates of complex vertexes depend on the same scale factor – reflection parameter β, the variable scaling is reasonable for practical problems in order to obtain comparable values;

– although the method of complexes does not require objective function continuity since it does not use derivative values, the function definition area needs to be convex, otherwise in some cases converging of the method is not provided. Such cases are unlikely in practice and using method normally gives good results.

References

[1] **John Vig R.** Quartz crystal resonators and oscillators for frequency control and timing applications – a tutorial. IEEE International Frequency Control Symposium Tutorials, 2004.

[2] **Lam C.** A review of the recent development of MEMS and crystal oscillators and their impacts on the frequency control products industry. IEEE Ultrasonics Symposium, Beijing, China, 2008, p. 694-704.

[3] **Taranchuk A., Pidchenko S., Skovryha O.** Pressure transducer based on the dual-mode piezoresonant sensors with modulated interelectrode gap. Proceedings of IEEE 36th International Conference on Electronics and Nanotechnology, Kiev, Ukraine, 2016, p. 261-263.

[4] **Pidchenko S.** Dual-frequency temperature-compensated Quartz Crystal Oscillator. Proceedings of IEEE 23th International Crimean Conference on Microwave and Telecommunication Technology, Sevastopol, Crimea, Ukraine, 2013, p. 669-670.

[5] **Bargin V., Zelensky A., Kolpakov F., et al.** multi-mode quartz resonator-thermosensor. Electronic Engineering. Radio-Components, Vol. 10, Issue 2, 1972, p. 54-57, (in Russian).

[6] **Pidchenko S.** Theory and Fundamentals Implementation of Invariant Piezoresonance Devices and Systems. KNU, Khmelnytskyi, 2014, p. 400.

[7] **Mensky B.** The Principle of Invariance in Automatic Regulation and Control. Mashinostroenie, 1972, p. 248, (in Russian).

[8] **Kharkevich A.** Favourites Proceedings, Vol. 1, Nauka, 1973, p. 400, (in Russian).

[9] **Pidchenko S., Taranchuk A., Spivak A., Akulynichev A.** The technical invariance of piezoresonance devices of the info communication systems. Proceedings of IEEE 3rd International Scientific-Practical Conference Problems of Info Communications Science and Technology, Kharkiv, Ukraine, 2016, p. 71-72.

[10] **Pidchenko S., Taranchuk A., Totsky A., Akulynichev A.** Providing of invariance property for piezo resonance devices on the basis of adaptive systems contained predictive standard. Proceedings of IEEE 4rd International Scientific-Practical Conference Problems of Info Communications Science and Technology, Kharkiv, Ukraine, 2016, p. 572-575.

[11] **Krasovskii A., Bukov V., Shendrik V.** Universal Algorithms for Optimal Control of Continuous Processes. a Series of Theoretical Foundations of Technical Cybernetics. Nauka, Moscow, 1977, p. 272.

[12] **Pidchenko S., Taranchuk A.** Principles of quartz multi-frequency oscillatory systems with digital compensation of temperature and vibrational instability frequency. Proceedings of IEEE International Conference Radio Electronics and Info Communications, Kiev, Ukraine, 2016, p. 281-284.

[13] **Zelenskiy A., Pidchenko S., Taranchuk A.** Multifrequency core structure of an invariant quartz oscillatory system. Proceedings of IEEE 11th International Conference on Modern Problems of Radio Engineering, Telecommunication and Computer Science, Lviv-Slavske, Ukraine, 2012, p. 125.

[14] **Taranchuk A., Pidchenko S., Khoptinskiy R.** Dynamics of temperature-frequency processes in multifrequency crystal oscillators with digital compensations of resonator performance instability. Radioelectronics and Communications Systems, Allerton Press Inc. USA, Vol. 58, Issue 6, 2015, p. 250-257.

[15] **Pidchenko S., Taranchuk A., Totsky A.** Multi-frequency quartz oscillating systems using digital compensation of frequency instability caused by variations of temperature and vibrations. Begell House Inc., USA, Vol. 76, Issue 13, 2017, p. 1193-1200.

[16] **Reklaitis G., Ravindrank A., Ragsdell M.** Engineering Optimization: Methods and Applications. John Wiley and Sons, 1983.

Sergey Pidchenko, D.Sc., Associate Professor in Department of Telecommunication and Computer-Integrated Technologies at Khmelnytsky National University. The field of scientific interests includes the problems of generating, forming and processing highly stable multi-frequency signals in info communication systems. Author of more than 120 publications in this field of research.

Alla Taranchuk, Ph.D., Associate Professor in Department of Telecommunication and Computer-Integrated Technologies at Khmelnytsky National University. The field of scientific interests includes the problems of generating, forming and processing highly stable multi-frequency signals in telecommunication systems. Author of more than 80 publications in this field of research.